Submitted to ***Lithos***

Geochronology and geochemistry of Late Paleozoic magmatic rocks in the Lamasu-Dabate area, northwestern Tianshan (west China): evidence for a tectonic transition from arc to post-collisional setting

Gong-Jian Tang[a, b], Qiang Wang[a*, c], Derek A. Wyman[d], Min Sun[e], Zheng-Xiang Li[c], Zhen-Hua Zhao[a], Wei-Dong Sun[a], Xiao-Hui Jia[a, b], Zi-Qi Jiang[a, b]

[a] Key Laboratory of Isotope Geochronology and Geochemistry, Guangzhou Institute of Geochemistry, Chinese Academy of Sciences, Guangzhou 510640, P. R. China

[b] Graduate University of Chinese Academy of Sciences, Beijing 100049, China

[c] The Institute for Geoscience Research (TIGeR), Department of Applied Geology, Curtin University of Technology, GPO Box U1987, Perth, WA 6845, Australia

[d] School of Geosciences, Division of Geology and Geophysics, The University of Sydney, NSW 2006, Australia

[e] Department of Earth Sciences, The University of Hong Kong, China

***Corresponding author**

E-mail address: wqiang@gig.ac.cn (Q. Wang)

Abstract

Voluminous Late Paleozoic igneous rocks and associated Cu-Au-Mo deposits occur in the northwestern Tianshan district, Xinjiang, west China. However, the tectonic setting and petrogenesis of these rocks remain controversial. This paper reports zircon U-Pb and Hf isotopic data, major and trace elements, and Sr–Nd–Pb isotopic data for the intrusive rocks and minor dacites in the Lamasu-Dabate area of northwestern Tianshan adjacent to the Cu-Au-Mo deposits. LA-ICPMS U–Pb zircon analyses suggest that the Lamasu porphyries were formed at 366 ± 3 Ma and contain 907-738 Ma inherited zircons, the Dabate dacites were formed at 316 ± 4 Ma, and granite porphyries were formed at 289 ± 3 Ma with ~ 319 Ma inherited zircons. The Lamasu porphyries consist of plagioclase granite and granodiorite, and are geochemically similar to adakites, e.g., having high Al_2O_3 (14.54-19.75 wt.%) and Sr (308-641 ppm) and low Y (7.84-16.9 ppm) contents, with fractionated rare earth element (REE) patterns and slightly positive Sr anomalies. However, they have variable initial ratios of $^{87}Sr/^{86}Sr$ (0.7072-0.7076) and $^{206}Pb/^{204}Pb$ (18.139-18.450), and variable $\varepsilon_{Nd}(t)$ (-5.6 to -0.8) and positive $\varepsilon_{Hf}(t)$ (+1.4 to +10.6) values. They also have variable $Mg^{\#}$ ($100\times Mg^{2+}/(Mg^{2+}+Fe^{2+})$) (41-73) and low Th (3.13-8.09) and Th/Ce (0.14-0.28) values. We suggest that the Lamasu adakitic magmas were generated through partial melting of southward subducted Junggar oceanic crust, with subsequent melt-mantle interaction and assimilation of basement rocks. The Dabate dacites show typical arc-like geochemical characteristics (e.g., enrichment of large ion lithophile elements (LILE) and strong negative anomalies of Ta, Nb, P and Ti), with variable $\varepsilon_{Nd}(t)$ (+0.1 to +3.3). They were probably generated by melting of juvenile basaltic lower crust as a result of magma underplating. The Dabate granite porphyries are geochemically similar to A_2-type granites, e.g., high SiO_2 (75.6-77.6 wt.%) and alkalis (Na_2O+K_2O = 8.27-8.70 wt.%), low CaO (0.28-0.34 wt.%) and $Mg^{\#}$ (2-10), and obvious negative Eu, Ba and Sr anomalies. They have variable values of $\varepsilon_{Nd}(t)$ (-1.7 to 0) and $^{206}Pb/^{204}Pb_i$ (18.567 - 18.721) and zircon $\varepsilon_{Hf}(t)$ (+0.5 to +11.1). The Dabate A-type granite porphyries contain Late Carboniferous residual zircon cores, suggesting that their source rock possibly contained Carboniferous arc igneous rocks. Taking into account all available data from Late Paleozoic magmatic rocks and Cu-Mo-Au mineralization in the northern Tianshan district, we suggest that the Dabate-Lamasu area was a continental arc

during the Late Devonian-Carboniferous but had entered a post-collisional stage by the Early-Permian (~ 290 Ma).

Key words: Adakite; A-type granite; arc; post-collisional; Xinjiang; Central Asian Orogenic Belt

1. Introduction

Recognizing tectonic transitions from convergent margins to post-collision settings is an interesting and an important challenge for geodynamic studies (e.g., Liégeois et al., 1998; Ma et al., 1998; Barbarin, 1999; Chung et al., 2005; Whalen et al., 2006; Guo et al., 2007). One common approach is to use changes in the characteristics and types of magmatic rocks to establish the change in tectonic regimes (e.g., Barbarin, 1999; Chung et al., 2005). For instance, adakites are often considered to have been generated in arc settings (e.g., Defant and Drummond, 1990; Martin et al., 2005), whereas A-type granites are commonly linked to rift or post-collisional settings (Eby, 1990, 1992; Whalen et al., 1987) or a mildly extensional back-arc setting inboard of the continental margin arc (Rivers and Corrigan, 2000). Such interpretations are not always straightforward.

The northwestern Tianshan Orogenic Belt (NTOB) is characterized by widespread igneous rocks consisting predominantly of Late Paleozoic granites, intermediate volcanic rocks and minor mafic intrusions (Fig. 1). These igneous rocks have attracted much attention because they are often associated with Cu-Au-Mo mineralization. However, the tectonic setting for the magmatism is still a matter of debate. Two types of models have been proposed in the last decade. Some researchers suggested an extensional setting for the Late Paleozoic (e.g., Carboniferous-Permian) igneous rocks, such as an intra-continental rift (Xia et al., 2004a), a post-collisional environment (Wang and Xu, 2006; Han et al., 2010) or a mantle plume (Xia et al., 2004b; Zhou et al., 2004; Pirajno et al., 2008). Conversely, others suggested that the Late Paleozoic tectonic setting of the NTOB was mainly related to subduction of the Junggar plate beneath the Yili-Central Tianshan plate (YCTP) (Gao et al., 1998; Liu and Fei, 2006; Wang et al., 2007c; Windley et al., 1990; Xiao et al., 2008, 2009, 2004; Zhou et al., 2004;). Proponents of the latter model also disagree on the timing and evolution of the NTOB, with the proposed timing for the final closure of the Junggar Ocean ranging from end of the Early Carboniferous (Gao et al., 1998; Geng et al., 2009; Yin et al., 2010), the end of the Late Carboniferous (e.g., Allen et al., 1993; Carroll et al., 1995; Coleman, 1989; Wang et al., 2006, 2007c; Han et al., 2010), or the Late Permian (Xiao et al., 2008).

There are numerous porphyry copper and epithermal gold deposits in the Tianshan district (Seltmann and Porter, 20005; Yakubchuk, 2004), e.g., the Tuwu-Yandong porphyry copper-gold deposit (4.7 Mt Cu and 19 t Au; Zhang et al., 2006a) and the Axi (50 t Au) (Zhai et al., 2009) and Jinxi-Yelmand (60 t Au) epithermal gold deposits (Xiao et al., 2005). All of these deposits were formed during the Late Devonian-Late Carboniferous interval and were associated with contemporary igneous rocks (e.g., Qin et al., 2002; Wang et al., 2006c; Zhang et al., 2006a). Although a number of detailed studies have been conducted on the geology and timing of some of the deposits (Zhang et al., 2006b, 2008b, 2008c), relationships between ore genesis and magmatism, and tectonic settings remain unclear.

In this paper we report zircon U-Pb ages, and geochemical, Sr-Nd-Pb and zircon Hf isotopic compositions of the Lamasu and Dabate magmatic rocks in the NTOB. The studied rocks include adakitic granitoids, dacites with ‘arc-like geochemical characteristics’, and A-type granites formed during the Late Devonian and the Early Permian, respectively. Based on these new data and previously published geological, geochronological, and geochemical data for porphyries in other NTOB Cu-Au deposits, we examine the petrogenesis of the Lamasu and Dabate magmatic rocks and the relationship between ore genesis and Late Paleozoic magmatism and tectonics in the region.

2. Geologic background

The NTOB is the north branch of the Tianshan Orogenic Belt (Fig. 1). It is located between the Junggar plate to the north and the Yili-Central Tianshan plate (YCTP) to the south (Fig. 1). It is widely accepted that the NTOB represents a Late Paleozoic continental arc developed along the northern margin of the YCTP due to the subduction of the Paleo-Junggar Ocean (e.g., Gao et al., 1998; Wang et al., 2007a, 2006c; Xiao et al., 2008).

The basement metamorphic rocks of the NTOB, consisting of Precambrian (821-798 Ma) granitic gneisses and amphibolites of the Wenquan Formation crop out south of the Sayram Lake (Hu et al., 2000) (Fig. 1). Cambrian-Ordovician rocks mainly occur in the vicinity south-east of the Sayram Lake and consist of cherts, siltstones and carbonates. Silurian rocks are distributed along the southern side of the northern Tianshan Fault (NTF) and include flysches, limestones and intercalated calc-alkaline volcanic and volcano-sedimentary rocks (Wang et al., 2007a) (Fig. 1). Devonian rocks consist of conglomerates, sandstones, siltstones, basalts and andesitic porphyries, and mainly crop out in the Alataw and Bayingou area. Carboniferous strata are widespread in the NTOB and consist of limestone, sandstones, shale and volcanic rocks. Permian terrestrial sandstones and conglomerates in the Alataw and Sayram Lake area unconformably overlie all older rocks.

Late Devonian to Early Permian granitic and volcanic rocks occur along the NTOB with a west-northwest trend and minor Early Paleozoic granites are found in the Wenquan area (Fig. 1a, b). The Devonian to Carboniferous volcanic rocks mainly comprise calc-alkalic basalts, andesites and rhyolite flows, and tuffs (Xinjiang Bureau of Geology and Mineral Resources (XBGMR), 1993). Some Permian intrusive rocks also occur in the NTOB (XBGMR, 1993).

The NTOB hosts a large number of porphyry copper (molybdenum) and epithermal gold deposits (Li et al., 2006; Zhang et al., 2006b). The widespread porphyry copper deposits are associated with some of the Devonian to Late Carboniferous igneous rocks in the Lamasu-Dabate and Lailisigao’er areas (Fig. 1a, b). However, epithermal gold deposits mainly occur in the Axi area and are associated with Early Carboniferous andesites (Fig. 1a, b).

The Lamasu-Dabate area, northwest of the Sayram Lake, is located in the west part of the NTOB (Fig. 1a, b). Devonian to Carboniferous volcanic-sedimentary rocks are abundant. The Precambrian rocks exposed west of the Sayram Lake consist of grey limestone, mudstones and clastic rocks of the Neoproterozoic Kusongmuqieke Formation (XBGMR, 1993). The south Lamasu fault crops around 2 km to the south of the Lamasu and can be traced for more than 20 km (Fig. 1b).

The Lamasu Cu deposit is located about 3 km west of the Sayram Lake within variably recrystallised limestone of the Neoproterozoic Kusongmuqieke Formation, intruded by Late Paleozoic porphyry stocks (Fig. 1c). The ore-related porphyries consist of plagioclase granites, granodiorites and dioritic porphyries and diabases (Fig. 1c). The ore-bodies are mainly distributed along the contact zones between the porphyritic intrusions and limestone but some occur in fractures within the limestone. Numerous diabase dikes, typically 100 m long and 1-6 m wide, occur in the ore bodies (Fig. 1c) (Zhang et al., 2008c).

The Dabate Cu-Mo deposit is located about 20 km northeast of Sayram Lake within tuffaceous breccia and lava of the Devonian Tuosikuertawu Formation (Fig. 1d). Copper-Mo mineralization occurs mainly in dacites and the fracture zone between dacites and rhyolitic tuff breccia in the southwest of the Dabate area, rather than in the Dabate granites (Fig. 1d). A Re-Os age of 301 ± 20 Ma was reported for molybdenite in the Dabate deposit (Zhang et al., 2006c).

3. Petrography

There are a large number of intermediate-felsic intrusive bodies and dykes intruding the Neoproterozoic Kusongmuqieke Formation in the Lamasu area, which mainly consist of plagioclase granite and granodiorite. These rocks consist mainly of medium-fine to coarse-grained plagioclase, and minor quartz, biotite, and hornblende phenocrysts. Plagioclase crystals exhibit zonal textures and most exhibit some degree of sericitization. Quartz crystals commonly display rounded shapes due to resorption. Some altered porphyry samples contain biotite crystals that have been altered to chlorite, particularly along cleavages and grain boundaries. The plagioclase granite porphyries contain over 50 volume percent of phenocrysts whereas the granodiorite porphyry consists of less than 50 volume percent phenocrysts. In addition, the dominant phenocrysts for the plagioclase granite porphyry are plagioclase, hornblende, and biotite with minor quartz, but in granodiorite porphyry plagioclase, biotite and quartz phenocrysts are common.

Dacites in the Dabate area also exhibit a porphyritic texture with phenocrysts of plagioclase (10-15 vol. %), quartz (2-3 vol. %), hornblende (2-5 vol. %), and biotite (1-2 vol. %). Their groundmass is mainly composed of plagioclase (45-50 Vol. %) and quartz (25-30 vol. %). Plagioclase phenocrysts are euhedral, exhibiting zonal textures and variable degrees of sericitization. Quartz displays rounded shapes caused by resorption. Hornblende occurs as variably altered euhedral 50-200 μm phenocrysts, and 100-200 μm subhedral brown biotite phenocrysts also present.

The granite porphyries in the Dabate area typically contain coarse-grained (3-7 mm) phenocrysts of alkali-feldspar and quartz with subordinate biotite and plagioclase feldspar. Alkali-feldspar phenocrysts are generally subhedral or euhedral and some occur in polysyntheti or carlsbad-albite compound twins. Some quartz crystals show resorption shapes. The rims of some plagioclase phenocrysts exhibit sericitization. Biotite phenocrysts are generally platy with brownish color. The groundmasses mainly consist of quartz and potassium feldspar.

4. Results

Analytical methods, U-Pb age data, representative whole-rock geochemical analyses, Sr-Nd-Pb isotope data and *in situ* Hf isotopic analyses of zircons from the Lamasu and Dabate magmatic rocks are listed in Appendices 1-5, respectively. The least altered samples were selected for geochemical and isotopic analyses.

4.1 Zircon geochronology

To determine the emplacement ages of the porphyries, three samples were chosen for LA-ICPMS zircon U-Pb dating from the Lamasu and Dabate deposits. The zircon grains from the three samples have size ranges of 50–180 μm and 40–130 μm and length/width ratios of 2:1–3:1 and 1:1–3:1, respectively. Cathodoluminescence images of zircon grains used for LA-ICP-MS analysis show micro-scale oscillatory zoning with or without a homogeneous core (Fig. 2), and exhibit high Th/U ratios (0.12–1.07 for Lamasu samples and 0.45–1.32 and 0.28–1.01 for the Dabate dacite and granite samples, respectively), suggesting magmatic origins (Belousova et al., 2002). Concordia diagrams and representative CL images of analyzed zircons are shown in Fig. 2.

The Lamasu granodiorite porphyry sample (06XJ017) (Fig. 1, 80°58'43"N, 44°40'342"E): seventeen analyses of the youngest age population have indistinguishable U-Pb isotopic compositions, which correspond to a weighted mean $^{206}Pb/^{238}U$ age of 366 ± 3 Ma (2σ; MSWD = 0.28) (Fig. 2a). This age is interpreted as the best estimate of the time of crystallization of the Lamasu porphyries. Some zircons have core-rim structure and four analyses of zircon cores gave $^{206}Pb/^{238}U$ ages ranging between 738 Ma and 907 Ma, which either represent inheritance from the magma source or xenocrysts captured from Neoproterozoic country rocks. The remaining three analyses gave $^{206}Pb/^{238}U$ ages ranging between 400 ± 4 Ma and 405 ± 4 Ma for the zircon rims with a weighted mean $^{206}Pb/^{238}U$ age of 402 ± 5 Ma. The relatively old ages suggest that these zircons are inherited from the magma source or xenocrysts captured from country rocks.

The Dabate dacite sample (06XJ04) (Fig. 1, 81°25'25"N, 44°44'30"E): eight of twelve analyses have $^{206}Pb/^{238}U$ ages ranging from 310 ± 13 Ma to 325 ± 9 Ma, which correspond to a single age population with a weighted mean $^{206}Pb/^{238}U$ age of 316 ± 4 Ma (2σ) (MSWD = 0.33) (Fig. 2b). This age is considered to record the emplacement age of this intrusion. Some zircons also have core-rim structure and two analyses of zircon gave $^{206}Pb/^{238}U$ ages ranging between 774 Ma and 971 Ma, and the remaining two analyses of zircon gave $^{206}Pb/^{238}U$ ages about 420 Ma. These zircons may represent inheritance from the magma source or xenocrysts captured from country rocks.

The Dabate granite porphyry sample (06XJ013) (Fig. 1, 81°25'52"N, 44°44'45"E): eighteen of twenty-four analyzes have $^{206}Pb/^{238}U$ ages ranging from 278 ± 3 Ma to 294 ± 3 Ma, which correspond to a single age population with a weighted mean $^{206}Pb/^{238}U$ age of 289 ± 3 Ma (2σ) (MSWD = 2.3), which is taken here as the emplacement age of this intrusion. The remaining four analyses for cores and rounded zircons yielded a weighted mean $^{206}Pb/^{238}U$ age of 319 ± 6 Ma (Fig. 2c), which is interpreted to signify trapped grains from Carboniferous volcanic rocks.

4.2 Whole-rock geochemistry

4.2.1 The Lamasu intrusive rocks

The compositions of the Lamasu intrusive rocks range from gabbroic-dioritic to granitic, but are mainly granodioritic to granitic (Fig. 3a) and with sub-alkaline affinities (Fig. 3b). They are calc-alkaline and plot in the fields of medium- and high-K calc-alkaline series igneous rocks (Fig. 3c and d). The Lamasu intrusive rocks can be subdivided into three groups based on their petrography: plagioclase granite porphyries and granodiorite porphyries (group 1); diorite porphyries (group 2) and diabases (group 3). Chondrite-normalized REE patterns (Fig. 4a) for the three groups are approximately parallel, and their light and heavy rare earth elements (LREE and HREE) are enriched and depleted, respectively. The plagioclase granite and granodiorite porphyries have consistent geochemical compositions, with slightly negative Eu anomalies (Eu/Eu* ($Eu_N/[(1/2)\times(Sm_N+Gd_N)]$, where subscript N denotes chondrite normalized) = 0.52-0.74) (Fig. 4a; Table 1). Primitive mantle-normalized trace element patterns (Fig. 4b) show that the plagioclase granite and granodiorite porphyries have Nb, Ta and Ti depletions. The diorite porphyries display distinct negative Eu anomalies (Eu/Eu* = 0.50-0.52) and higher REE contents, whereas, the diabase porphyry has a positive Eu anomaly (Eu/Eu* = 1.22) (Fig. 4a). The diorite porphyries have negative Sr anomalies and no Ti anomalies, and the diabase has negligible Nb, Ta anomalies, a positive Ti anomaly and a slight depletion of large ion lithophile elements (LILE) (Fig. 4b).

The Lamasu plagioclase granite and granodiorite porphyries exhibit adakite geochemical characteristics (Defant and Drummond, 1990; Kay, 1978; Martin et al., 2005). These samples are characterized by fractionated rare earth element (REE) patterns (La/Yb_N = 4.6-10.6) (Fig. 4a, 5a; Table 1), and slightly positive Sr anomalies (Fig. 4b), though they have slightly negative Eu anomalies (Fig. 4a), with high Al_2O_3 (14.54-19.75 wt.%), Sr (308-641 ppm) and lower Y (7.84-16.9 ppm) contents (Table 1). On the Sr/Y-Y discrimination diagrams of Defant and Drummond (1990) (not shown), they plot in the adakite field, and they are similar to Tuwu-Yandong adakitic porphyries, though with slightly higher Yb_N (Fig. 5a). The diorite porphyries (06XJ19-1 and 06XJ19-2) do not show adakitic geochemical characteristics and have relatively lower Sr contents (131-257 ppm) and Sr/Y ratios (6-11) (Appendix 3).

4.2.2 The Dabate dacites

The Dabate dacite samples have consistent geochemical signatures (Fig. 3). They have SiO_2 contents of 62.12 to 64.38 wt.% (Table 1), and display sub-alkaline affinities on a Nb/Y-Zr/Ti diagram (Fig. 3b) and calc-alkaline affinities on the AFM plot (Fig. 3c). The dacite samples fall in the field of medium and high K calc-alkaline igneous rocks (Fig. 3d). They are metaluminous or peraluminous with A/CNK (molar [Al/(Ca +Na + K)] = 0.96 - 1.22), display LREE enrichment and HREE depletion ($(La/Yb)_N$ = 3.3-6.4) with slightly negative Eu anomalies (Eu/Eu* = 0.55-0.83) (Fig. 4c; Table 1). These rocks are characterized by strong negative anomalies of Ta, Nb, P and Ti, and enrichment in LILE in primitive mantle-normalized diagram, suggesting a typical arc-like nature (Tatsumi and Eggins, 1995) (Fig. 4d). Overall, these rocks show characteristics similar to others previously attributed to Late Carboniferous arc magmatism on the north margin of the YCTP (Wang et al., 2007a, 2007c).

4.2.3 The Dabate granite porphyries

The Dabate granite porphyries have high SiO_2 (73.97-77.61 wt.%) and K_2O (4.92–8.08 wt%) contents, high K_2O/Na_2O ratios (1.2–5.8) (Table 1; Appendix 3) and low Al_2O_3 contents (12.0-13.1 wt.%), and exhibit weakly metaluminous to peraluminous characteristics (A/CNK = 0.93-1.55). They are low in CaO, MgO and P_2O_5 and plot in the field of high-K calc-alkaline igneous rocks (Fig. 3d). The porphyries also show relatively flat normalized REE patterns $(La/Yb)_N$ = 1.6-5.2) with pronounced negative Eu anomalies (Eu/Eu* = 0.09-0.19) (Fig. 4e; Table 1). They have high concentrations of high field strength elements HFSE (Zr, Hf, Nb and Ta) and LILE (Th and U) (Fig. 4f) and strong negative Sr, Ba and Ti anomalies.

The Dabate granite porphyries in the NTOB are geochemically similar to typical A-type granites (Eby, 1990, 1992; Frost et al., 2001; Whalen et al., 1987). They have high total alkalis contents (K_2O+Na_2O = 8.26-10.10 wt.%) and FeO_{total}/(FeO_{total}+MgO) ratios (0.77-0.99). The extremely low P_2O_5 contents and the absence of any phosphate mineral also suggest that the Dabate granitic porphyries are similar to A-type granites rather than S-type leuogranites (Bonin, 2007; King et al., 1997). The trace element composition of the Dabate granitic porphyries also exhibits A-type granite geochemical characteristics (Whalen et al., 1987; Wu et al., 2002), e.g., high 10,000×Ga/Al ratios (3.7–4.2, with an average value of 3.7 (Appendix 3), enrichment in HFSE (Nb, Y and Zr), no Nb-Ta anomalies, and clear depletions in Ba, Sr, Eu and Ti (Fig. 4f). They also have Nb/Ta (10-13) and Zr/Hf (22-28) ratios similar to typical A-type granite (Eby, 1992; King et al., 1997). They plot in the A-type granite field on discrimination diagrams involving Ga/Al (Fig. 6) and in the within-plate field on Y-Nb and Ta-Yb plots (Fig. 7a-b). They also have high Yb/Ta (1.5–3.9) and Y/Nb (1.43–3.51) ratios, suggesting that they can be further classified as A_2-type granites (Eby,1992) (Fig. 7c-d).

4.3 Sr-Nd-Pb isotopic geochemistry

Initial $^{87}Sr/^{86}Sr$ ratios and $\varepsilon_{Nd}(t)$ values were calculated using the new age data. Because the Dabate granite porphyries have extremely high Rb/Sr ratios, their calculated initial $^{87}Sr/^{86}Sr$ ratios are not meaningful (e.g., Wu et al., 2002). The Lamasu plagioclase granites and granodiorite porphyries have initial $^{87}Sr/^{86}Sr$ ratios ranging from 0.7072 to 0.7076 and negative $\varepsilon_{Nd}(t)$ values ranging from -3.7 to -0.8. One diabase sample has lower initial $^{87}Sr/^{86}Sr$ ratio (0.7059) and positive $\varepsilon_{Nd}(t)$ value (+3.4). A diorite porphyry sample also has a positive $\varepsilon_{Nd}(t)$ value of +1.4 (Appendix 4; Fig. 8a). The Dabate dacites have variable $\varepsilon_{Nd}(t)$ value ranging from +0.1 to +3.3. The Dabate granite porphyries have slightly higher $\varepsilon_{Nd}(t)$ value (-1.7 to 0.0) than those of the Lamasu plagioclase granites and granodiorite porphyries (Fig. 8a).

The Lamasu plagioclase granite and granodiorite porphyries and the Dabate granite porphyries have radiogenic Pb isotopic compositions with $^{206}Pb/^{204}Pb_i$ ranging from 15.538-15.581 and 15.635-15.717, respectively (Appendix 4; Fig. 8b). The Lamasu diorite and diabase porphyries have $^{206}Pb/^{204}Pb_i$ values of 18.046 and 17.909, respectively (Fig. 8b), and two Dabate granite porphyry samples have similar Pb isotopic compositions with $^{206}Pb/^{204}Pb_i$ and $^{207}Pb/^{204}Pb_i$ values of 18.569-18.721 and 15.714-15.717, respectively (Appendix 4; Fig. 8b)

4.4 Zircon Hf isotopic geochemistry

In situ Hf isotopic analyses of zircons from the Lamasu granodiorite porphyry and Dabate granite porphyry samples are shown in Figures 8c and 9. Three groups of zircons are recognized from the Lamasu granodiorite porphyry sample (06XJ17). The magmatic zircons with 366 Ma crystallization ages (group 1) have variable Hf isotopic compositions (Appendix 5; Fig. 9a), with $^{176}Hf/^{177}Hf$ ratios of 0.282594-0.282865, $\varepsilon_{Hf}(t)$ values of +1.4 to +10.6 and T_{DM} values of 0.58–0.95 Ga. The group 2 entrained zircons (400-405 Ma) have $^{176}Hf/^{177}Hf$ ratios of 0.282574–0.282606, $\varepsilon_{Hf}(t)$ values of +0.8 to +1.7 and T_{DM} values of 0.93–0.96 Ga (Appendix 5; Fig. 9a). The inherited zircon cores (738-907 Ma) (group 3) have variable Hf isotopic compositions, with $^{176}Hf/^{177}Hf$ ratios of 0.282529-0.282779, $\varepsilon_{Hf}(t)$ values of -9.7 to -0.9, and T_{DM} values of 1.04–1.39 Ga (Appendix 5; Fig. 9a).

Magmatic zircons (group 1) from the Dabate granite porphyry sample (06XJ13) also have variable Hf isotopic compositions with $^{176}Hf/^{177}Hf$ ratios of 0.282624–0.282883, $\varepsilon_{Hf}(t)$ values of +0.5 to +8.3 and T_{DM} values of 0.6-0.9Ga (Appendix 5; Fig. 9b). However, three xenocrystic zircons (group2, ca.319 Ma) from this sample have $^{176}Hf/^{177}Hf$ ratios of 0.282694–0.282926, $\varepsilon_{Hf}(t)$ values of +3.0 to +11.1 and T_{DM} values of 0.49-0.81 Ga (Appendix 5; Fig. 9b).

5. Discussion

5.1. Three episode*s of magmatic rocks in the NTOB*

The available data clearly show three main magmatic episodes in the Late Paleozoic for the NTOB (Fig. 10). The first episode occurred during the Late Devonian to the Early Carboniferous (366-341 Ma). Typical examples include: (1) the 362-350 Ma Lailisigao'er granodiorite porphyry and monzodioritic porphyritic plutons associated with Cu-Mo deposits (Li et al., 2006; Zhang et al., 2009); (2) ~ 345 Ma intrusive rocks associated with copper mineralization located 1 km to the northwest of the Lailisigao'er Cu-Mo deposits (Fig. 1); (3) the ~ 352 Ma Guozigou granodiorite (Xu et al. 2006b); (4) the ~ 363 Ma volcanic rocks of the Dahalajunshan formation in the Axi low-sulfidation type epithermal gold deposit (Zhai et al. 2006; 2009); and (5) the ~ 366 Ma Lamasu plagioclase granite porphyry (this study), which formed in an arc setting. The second episode of magmatism occurred during the Late Carboniferous (317-306 Ma). Typical examples include: (1) the ~ 316 Ma Dabate dacite (Zhang et al., 2008b); (2) ~ 317 Ma Kekesai granodiorite porphyry (Zhang et al., 2008a); (3) the ~ 308 Ma Borohoro diorite pluton (Zhu et al., 2006)); (3) the 310-306 Ma Alatawa adakites (Wang et al., 2007c). This magmatic episode most probably occurred in an arc setting associated with the southward subduction of the Junggar Ocean (Wang et al., 2007a, 2007c). The youngest magmatism is of Early Permian age (294-280 Ma). The A-type Dabate granitic porphyry (289 ± 3 Ma, this study) is typical of this magmatic episode. The high-K calc-alkaline granites of the Borohoro area (Fig. 1) have a similar age (294–280 Ma) and have been interpreted to have formed in a post-collisional setting (Wang et al., 2009).

In the study region, the three episodes of magmatism are represented by the 366 ± 3 Ma Lamasu granodiorite porphyries (this study), the 316 ± 4 Ma (this study) and the 316 ± 6 Ma Dabate dacite (Zhang et al., 2008b), and the Dabate A-type granites, respectively. These three episodes of magmatic rocks possibly recorded the changes in tectonic settings in the NTOB.

5.2 Petrogenesis

5.2.1 The Lamasu intrusive rocks

Except for slightly negative Eu anomalies, most samples of the Lamasu granites and granodiorite porpyries exhibit geochemical characteristics of adakites. Adakites were originally considered to be generated by melting of subducted young and hot oceanic crust (Model A) (Defant and Drummond, 1990), based on a study of magnesian andesite from Adak Island in the Aleutians (Kay, 1978). They have been extensively studied because of their unusual compositions, tectonic settings and potential for Cu-Au mineralization (e.g., Defant and Kepezhinskas, 2001; Martin et al., 2005; Mungall, 2002; Oyarzun et al., 2001; Reich et al., 2003; Wang et al., 2006b).

We suggest that the Lamasu adakitic magmas were most probably generated by partial melting of subducted oceanic crust based on both geological and geochemical evidence. First, there is growing evidence for a Devonian to Early Carboniferous arc setting in the northwestern Tianshan. Recently, some Carboniferous ophiolites have been identified in the area, e.g., the 344.0 ± 3.4 Ma Bayingou ophiolite in the northwestern Tianshan (Xu et al., 2006a). This ophiolite is only slightly younger than the Lamasu intrusive rocks. Devonian to Early Carboniferous arc-type granitoids and volcanic rocks are abundant in this region (Fig. 1). Many studies suggest that a Junggar oceanic crust subducted south beneath the YCTP, forming a Late Devonian to Early Carboniferous arc along the northern margin of the YCTP (Gao et al., 1998; Liu and Fei, 2006; Wang et al., 2007c; Windley et al., 1990; Xiao et al., 1991). Kröner et al. (2008) described Late Palaeozoic (407-369 Ma) granitoids in central Kazakhstan (the westward extension of northwestern Tianshan) and showed that they are the product of arc magmatism. The Lamasu intrusive rocks exhibit Nb, Ta and Ti depletions and enrichment of mobile LILE, similar to arc-related magmatism (Tatsumi and Eggins, 1995) (Fig. 4b). On the Y-Nb and Yb-Ta tectonic discrimination diagram (Fig. 7a-b) (Pearce et al., 1984), all samples of the Late Devonian to Early Carboniferous porphyries in the Lamasu and Lailisigao'er areas plot in the volcanic arc field. These studies suggest that there was an active margin during the Devonian to Early Carboniferous in the study region and that the Lamasu adakitic rocks formed in an arc setting. Second, the Lamasu intrusive rocks are geochemically similar to slab-derived adakites. Although some samples of the Lamasu intrusive rocks have low MgO contents (Fig. 5c), most samples have high $Mg^{\#}$ values (Fig. 5d), similar to those of typical subducted oceanic crust-derived adakite. In addition, they have very low Th contents (3.13-8.09 ppm) and low Th/Ce ratios (0.14-0.28), indicating that their compositions are more consistent with Cenozoic adakite formed by slab melting in an arc setting (Defant et al., 1992; Kay, 1978; Kay et al., 1993; Stern and Kilian, 1996; Moyen and Stevens, 2006).

However, the Lamasu intrusive rocks show slightly negative Eu anomalies (Eu/Eu* = 0.52 - 0.74) (Fig. 4a; Table 1), in contrast to typical subducted oceanic crust-derived adakites that have negligible-positive Eu anomalies (Defant and Drummond, 1990). The negative Eu anomalies of the Lamasu intrusive rocks may be caused by three processes: (1) fractional crystallization of plagioclase; (2) residual plagioclase in the source; (3) crustal contamination. On a plot of Nb/Ta versus Zr/Sm (Fig. 5b) the Lamasu intrusive rocks fall in the field of hornblende eclogite melting rather than that of rutile eclogite. This suggests that the Lamasu adakitic rocks were generated at shallower depths, and thus minor plagioclases might be stable as residual phases. It may also be possible that the Nb/Ta fractionation occurs during dehydration of subducting slabs under thermal gradients (Xiao et al., 2006; Ding et al., 2009; Liang et al., 2009). The depleted HREE and Y (Fig. 4a-b) suggest that garnet was a major residual mineral in their source.

The Lamasu intrusive rocks have more variable and higher initial $^{87}Sr/^{86}Sr$ ratios, lower εNd(t) values and more variable MgO contents than slab-derived adakites (Fig. 8; Appendix 4), but high $Mg^{\#}$ similar to the latter (Fig. 5d). These characteristics may reflect two-stage contamination: slab-derived melts were first contaminated by mantle peridotite during ascent, increasing MgO, $Mg^{\#}$ and compatible elements contents (Fig. 5d); followed by contamination by basement metamorphic rocks during passage through the crust. This scenario is strongly supported by inherited zircons with northwestern Tianshan Neoproterozoic basement crust ages (900 ± 20 Ma; Fig. 2a) (Hu et al., 2000) in the Lamasu adakites. The presence of Neoproterozoic zircon xenocrysts and their negative εHf values strongly suggests that basement crustal contamination also played a significant role in the formation of the Lamasu intrusive rocks. Crustal contamination would also decrease MgO, $Mg^{\#}$ and εNd(t) values, increase initial $^{87}Sr/^{86}Sr$ ratios, and contribute to the large variations observed in these values. Collectively, the evidence suggests that a combination of crustal assimilation and fractional crystallization (AFC) were involved in the petrogenesis of the Lamasu intrusive rocks. The process is isotopically modeled in Figure 12. A Neoproterozoic basement crust was selected with 60 ppm Sr, 40 ppm Nd, $(^{87}Sr/^{86}Sr)_i$ of 0.7206 and $\varepsilon_{Nd}(t)$ value of - 8.31 [$(^{143}Nd/^{144}Nd)_i$ = 0.51248] (Hu et al., 2000). The original magma of the Lamasu intrusive rocks is inferred to have been derived from source rocks similar to the gabbros of the Bayingou ophiolites (Xu et al., 2006a), with 127 ppm Sr, 6 ppm Nd, $(^{87}Sr/^{86}Sr)_i$ of 0.7036 and $\varepsilon_{Nd}(t)$ value of +5.0 [$(^{143}Nd/^{144}Nd)_i$ = 0.51174]. On a $(^{143}Nd/^{144}Nd)_i$ versus $(^{87}Sr/^{86}Sr)_i$ plot (Fig. 12a), an AFC trend with an assimilation rate (r) of 0.3 passes through the middle of the isotopic range defined by the Lamasu intrusive rocks.

The genesis of adakites, however, is still a matter of debate, and a number of other genetic models have been proposed, for example: (a) partial melting of thickened basaltic lower crust (Model B) (e.g., Atherton and Petford, 1993; Chung et al., 2003; Condie, 2005; Wang et al., 2005, 2007b); (b) partial melting of delaminated lower crust (Model C) (e.g., Kay and Kay, 1993; Xu et al., 2002; Gao et al., 2004; Wang et al., 2007b, 2006b; Xiao and Clemens, 2007; Zhang et al., 2007); (c) crustal assimilation as well as fractional crystallization from parental basaltic magmas (Model D) (e.g., Castillo et al., 1999; Macpherson et al., 2006; Richards and Kerich, 2007). We consider these alternative processes below with specific reference to the Lamasu adakitic porphyries.

The geochemical characteristics of the Lamasu intrusive porphyries are inconsistent with partial melting of thickened continental lower crust (Models B). Commonly, adakitic rocks derived by melting of thickened lower crust are characterized by relatively low MgO or $Mg^{\#}$ values (Fig. 5c-d), which are similar to those of experimental melts from metabasalts and eclogites (Rapp et al., 1999; Rapp and Watson, 1995; Sen and Dunn, 1994). The Lamasu intrusive rocks, however, display distinctly higher $Mg^{\#}$ values than the experimental melts, although they have low MgO contents (Fig. 5c-d) (Rapp et al., 1999). Moreover, adakitic rocks formed by Model B generally have higher K_2O contents and are high-K calc-alkaline (Atherton and Petford, 1993; Muir et al., 1995; Wang et al., 2005, 2007b), but some of the Lamasu samples have lower K_2O content and are calc-alkaline (Fig. 3d).

Based on their geochemical characteristics, high $Mg^{\#}$ values (Fig. 5d) and relatively low εNd values (Fig. 8a), it might be argued that the Lamasu intrusive porphyries could have been generated by partial melting of delaminated lower crust (Model C). In general, however, adakitic rocks formed by delamination occur in within-plate setting and are associated with contemporary within-plate or extension-related magmatic rock types (e.g., A-type granites) (Gao et al., 2004; Wang et al., 2006b). The northwestern Tianshan area is regarded as an active continental margin from the Late Devonian to the Early Carboniferous (Xiao et al., 2008). Late Devonian to Early Carboniferous arc volcanic rocks and granitoids occur widely in northwestern Tianshan and the Lamasu intrusive porphyries were not associated with contemporary within-plate or extension-related magmatic rocks (Long et al., 2008; Wang et al., 2009, 2006a, 2007c, 2006c) (Fig. 1). Given that Devonian to Carboniferous calc-alkaline volcanic rocks and deep marine volcanogenic sedimentary rocks dominate the northern Tianshan (Fig. 1) (Carroll et al., 1995), it seems unlikely that delamination of the lower crust took place in the Western Tianshan during the Late Devonian.

It is also unlikely that fractional crystallization from parental basaltic magmas (Model C) could account for the Lamasu intrusive porphyries. The most probable candidate for a basaltic parental magma would be the Lamasu diabase. If olivine and pyroxene fractionated from the diabase, then the derived magma would show a clear decrease in MgO contents and $Mg^{\#}$ values with increasing SiO_2 (Fig. 5c-d). However, the samples for the Lamasu intrusive porphyries do not plot along this trend on a SiO_2 versus $Mg^{\#}$ diagram (Fig. 5d). In addition, fractionation of olivine and pyroxene is inconsistent with the depletion of HREE (e.g., Yb) (Fig. 4a). This is because these minerals are incapable of incorporating HREE elements, and their formation would thus lead to concave-upward HREE in the chondrite-normalized REE concentration patterns instead (Castillo et al., 1999). Moreover, adakitic rocks formed by high-pressure fractional crystallization involving garnet generally display distinct geochemical characteristics (Macpherson et al., 2006), such as Al_2O_3 contents decreasing with increasing SiO_2, and Dy/Yb and Sr/Y ratios increasing with increasing SiO_2. However, the Lamasu adakitic rocks do not exhibit such trends. Al_2O_3/TiO_2 ratios vary between 32 and 91 for the Lamasu plagioclase granites, and between 35 and 55 for the Lamasu granodiorites (Fig. 11a). These variations are mainly controlled by Ti content (Fig. 11b). If the variations were entirely due to fractionation, then it could be caused by a minor Ti phase or a combination of major phases (plagioclase + hornblende?). A large change in Eu/Eu* (Fig. 11c) implies that plagioclase was involved (with other minerals) rather than just fractionation of a minor phase. Compatible major elements Fe and Mg decrease with increasing Al/Ti, (Fig. 11d-e), however, there is no clear trend between fractionation and Sr/Y (Fig. 11f). Similarly, the HREE do not support hornblende crystallization. Yb exhibits no trend or increases with Al/Ti and Gd displays a similar pattern (Fig. 11g-h). La/Yb also exhibits no clear trend but the highest Al/Ti value corresponds to the lowest La/Yb value (Fig. 11i), which is not consistent with control by hornblende fractionation.

In summary, the Lamasu adakitic rocks were most probably produced by partial melting of southward subducted oceanic crust in the Late Devonian (~366 Ma), followed by subsequent melt-mantle interaction and AFC by basement rocks.

5.2.2 The Dabate dacites

The Dabate dacites are intermediate in composition (SiO_2 = 62.12-64.38 wt.%) and mostly metaluminous to peraluminous based on the A/CNK range of 0.89-1.3. These calc-alkaline, intermediate volcanic rocks were considered to have been products of either fractional crystallization of mantle derived calc-alkaline basaltic magma (Barth et al., 1995), or partial melting of juvenile sub-alkaline metabasaltic rocks (e.g., Defant and Drummond, 1990; Rapp and Watson, 1995). Although the Dabate dacites have MgO concentrations similar to that of modern adakites produced by melting of subducted oceanic crust and subsequent interactions between slab melt and the mantle (e.g., Rapp et al., 1999) (Fig. 5c-d), coupled with significantly lower Sr/Y (4.1–21.5) and higher Y (19.3–41.4 ppm) and HREE (such as Yb = 1.7–4.0 ppm) than adakites (Table 1). Hence, the Dabate dacites are different in origin from adakites. Based on several lines of evidence below, fractional crystallization of basaltic magma can also be excluded. The Dabate dacites with large volumes of contemporaneous dacitic or dioritic magmatism, cannot be simply generated by fractional crystallization of basaltic magma. The Dabate dacite samples have nearly constant Al_2O_3 contents of 14.6-16.0 wt.% and relatively uniform REE and trace element abundances and patterns (Fig. 4c-d). Major and trace elements concentrations versus $Mg^{\#}$ or MgO plots (not shown) do not show systematic fractional crystallization trends from mafic to felsic magma.

The melting of a basaltic arc crust is a plausible mechanism for the petrogenesis of the Dabate dacites. In order to evaluate this process we use REE data for modeling of batch partial melting (Fig. 12b). Sample GNS30 of the Gongnisi basalt from northwestern Tianshan (Long et al., 2008) was selected as a proxy of juvenile lower crust beneath the NTOB. We assume that the partial melting took place under an amphibolite-facies condition and the initial mineralogical assemblages were Amph (amphibole): Plag (plagioclase): OPX (orthopyroxene) = 70:20:10. The chondrite-normalized REEs pattern for the Dabate dacites is reproduced by 25-35% batch melting. In addition, some of the Dabate dacites have MgO concentrations and $Mg^{\#}$ values (29-55) clearly higher than that of experimental melts (Fig.8c-d), indicating mantle-derived magmas were also possibly involved in the generation of the Dabate dacites. Therefore, we suggest that the Dabate dacites were generated by melting of juvenile basaltic lower crust, similar to the felsic calc-alkaline magmas from the southernmost Cascades, California (Borg and Clynne, 1998).

6.2.3 The Dabate A-type granite porphyries

It has been recognized that A-type granites can form in a variety of extensional tectonic environments, from continental back arc-extension to post-collision extension or within-plate tectonic settings (Eby, 1992; Förster et al., 1997; Turner et al., 1992; Whalen et al., 1987). The petrogenesis of a specific A-type granite is often controversial. Various genetic models invoke partial melting of crustal and mantle sources, fractional crystallization of basaltic compositions plus assimilation of crustal rocks and magma mixing (Collins et al., 1982; Eby, 1992; Kerr and Fryer, 1993; King et al., 1997; Whalen et al., 1987; Wu et al., 2002; Yang et al., 2006; Chen et al., 2009). Eby (1992) subdivided A-type granites into two sub-groups and suggested that they may have different origins and tectonic settings. The A_1-type granites represent differentiates of magmas derived from OIB-like sources emplaced in continental rifts or associated with intraplate magmatism, whereas the A_2-type granites are derived from melting of continental crust or underplated mafic crust that has been through a cycle of continent–continent collision or island-arc magmatism (Eby, 1992).

A purely crustal origin is untenable for the Dabate A-type granite porphyries (Bonin, 2007). On the one hand, the consistent slightly negative initial Nd isotopic compositions (εNd(t) = -1.72 to 0.00) of the Dabate A-type granite porphyries and the absence of inherited zircon with the Neoproterozoic ages preclude their derivation from melting of a highly evolved ancient continental crust, because the Neoproterozoic basement crust of the NTOB has negative Nd isotopic compositions ((εNd(t) = -8.5 – 11.7, Hu et al., 2000). On the other hand, positive zircon $\varepsilon_{Hf}(t)$ values (+0.5 to +8.3) of the Dabate A-type granite (Fig. 9b) imply a significant input of juvenile, mantle derived, material during magma generation and preclude a purely crustal origin. The Dabate A-type granite porphyries also could not have been produced by extreme differentiation of the Dabate dacites, because (1) there is a "Daly gap" between dacites and A-type granites; (2) all samples have a nearly constant Al_2O_3 content of 12–13% over the whole SiO_2 range (Appendix 3), and have consistent REE and trace element abundances and patterns (Fig. 4c-d).

The Dabate A-type granite porphyries contain late Carboniferous zircons (319-317 Ma) (Fig. 2b) that formed contemporaneously with the Dabate dacites (316 ± 6 Ma). Given that Late Carboniferous igneous rocks are widespread along the NTOB (Wang et al., 2006a; 2007c; 2006c) (Fig. 1 and 10), we suggest that the source of the Dabate A-type granite porphyries was a Late Carboniferous arc-related igneous protolith combined with the input of mafic magmas. The highest $\varepsilon_{Hf}(t)$ value of +11.7 calculated for inherited 319 Ma zircons, from sample 06XJ13 (Fig. 9b), is near the mantle value (Griffin et al., 2000). Therefore, the Dabate A-type granite porphyries were most likely generated by partial melting of a source rock which possibly contained an igneous rock formed during the late Carboniferous. Melting of this source rock was induced by mantle-derived hot mafic magmas during Early Permian crustal extension.

5.3 Coeval mineralization and magmatism in the northern Tianshan arc: Episodic metallogenic history

The new age data determined during this study as well as those reported previously indicate that the Cu-Mo-Au deposits within the NTOB (Fig. 1) are the product of discrete Late Devonian to Late Carboniferous events (Table 2).

Late Devonian to early Carboniferous gold-copper deposits are widespread throughout the northern Tianshan arc (Fig. 1). A typical example is the Lailisigao'er porphyry Cu-Mo deposit, which gave a 359 ± 8 Ma (Re-Os isochron) molybdenite (Li et al., 2006). This age is consistent with the 362-345 Ma ages of ore-related porphyries (Li et al., 2006; Zhang et al., 2009). The Lamasu porphyry Cu deposit and Axi low-sulfidation type epithermal gold deposit were both formed at this time (Table 2).

The Kekesai deposit (Zhang et al., 2008a) is an example of an NTOB porphyry Cu-Mo deposits formed during the Late Carboniferous (Fig. 1, Table 2). As noted above, the Dabate porphyry Cu-Mo deposit also has a molybdenite Re-Os isochron age of 301 ± 20 Ma (Zhang et al., 2006b). In addition, the Balkhash-Ili zone (Kazakhstan) in the western extension of the NTOB contains a number of late Carboniferous large tonnage porphyry deposits, including the 330 Ma Kounrad and the ~320 Ma Aktogai, Aidarly, Kyzilkia and Koksai porphyry deposits and the ~ 320 Ma Sayak skarn deposit (Seltmann and Porter, 20005).

No Early Permian Cu-Au deposits have been identified, although Early Permian intrusive rocks are common along the NTOB (Fig. 1). Given the ages summarized here, Cu-Au-Mo mineralization within the NTOB may have been episodic and associated with particular magmatic episodes during the Late Devonian to Early Carboniferous and the Late Carboniferous (Table 2). The idea of episodic mineralization is a preliminary one and further studies and an enlarged database are obviously required to test this hypothesis.

5.4 Tectonic evolution

The NTOB is a part of Central Asian Orogenic Belt, which has been the subject of numerous tectonic studies (e.g., Carroll et al., 1995; Gao et al., 1998; Sengör et al., 1993; Windley et al., 1990; Xiao et al., 2008). However, a consensus for the tectonic evolution of this orogenic belt has not been achieved. In the following section, we summarize the tectonic evolution of the northwestern Tianshan mainly based on data from Late Devonian to Early Permian igneous rocks (Fig. 13).

5.4.1. 455-345 Ma (Fig. 13a)

Late Devonian to Early Carboniferous (366-345 Ma) volcanic and plutonic rocks, including the Lamasu intrusive rocks, are sporadically distributed along northwestern Tianshan (Fig. 1 and 10) (Xu et al., 2006b; Zhai et al., 2006; Long et al., 2008; Wang et al., 2007a). Geochemically, they display Nb, Ta and Ti depletions and enrichment of mobile LILE, similar to subduction zone magmatism along the northwestern Tianshan (Fig. 1 and 4b). As with the Axi volcanic rocks (Long et al., 2008; Wang et al., 2007a), all of the Late Devonian to Early Carboniferous porphyries (Lamasu, Lailisigao'er and Axi) plot in the volcanic arc field on Y-Nb versus Yb-Ta tectonic discrimination diagrams (Pearce et al, 1984). These characteristics suggest that these porphyries may have been formed at an active continental margin. Recently, Hu et al., (2008) showed that medium- to coarse-grained amphibolites south of Wenquan were formed at 455.1 ± 2.7 Ma and 451.4 ± 5.7 Ma (zircon U-Pb ages), respectively, in an island-arc setting. These characteristics suggest that the initiation of southward subduction of the Junggar Ocean beneath the Yili - Central Tianshan block was present as early as the Late Ordovician, and the northwestern Tianshan continental arc magmatism and associated Cu or Au mineralizations were formed between the Late Devonian to the Early Carboniferous (Fig. 13a).

5.4.2. 345-320 Ma (Fig. 13b)

It is noteworthy that a magmatic gap or quiescent period existed between ca. 345 and 320 Ma after a period of continuous subduction that resulted in extensive Late Devonian to

Early Carboniferous magmatism (Fig. 10). We propose that, a period of "flat-subduction" can account for this ca. 345-320 Ma quiescence (Fig. 13b). In this model, mantle wedge asthenosphere was squeezed out by the flattening of the subducting slab, thus terminating arc magmatism (Kay and Mpodozis, 2001; Booker et al., 2004). An analogous mantle displacement process has been documented beneath the modern Central Andes (Kay and Mpodozis, 2001; Ramos and Folguera 2009) where flat subduction also occurs.

5.4.3. 317-306 Ma (Fig. 13c)

Subduction will generally revert from flat to normal angles once features such as topographic highs on the ocean floor or young crust generated at nearby spreading centres are no longer present. Such transitions are common in the geological record and numerous transitions between subduction angles are recognized in, for example, the Andes and central-south Tibet (Ramos and Folguera 2009, Ding et al., 2003; Wen et al., 2008; Lee et al., 2009). Before the final stage of closure of the Junggar Ocean, the oceanic slab is therefore likely to have undergone roll-back to normal, steeper, angles of slab subduction, induced asthenospheric convection and enhanced corner flow (Lee et al., 2009) (Fig. 13c). The continental arc setting in western Tianshan continued until the Late Carboniferous (Fig. 13c). Evidence for an active margin include gabbros and plagiogranites of the Bayingou ophiolite with zircon U-Pb ages of 344 ± 3 Ma and 325 ± 7 Ma, respectively (Xu et al., 2006a). Wang et al. (2007c, 2006c) described late Carboniferous adakite, high Mg andesite and Nb-enriched arc basalt suites in northwestern Tianshan similar to those in Cenozoic arcs, and suggested Carboniferous oceanic subduction along the northern margin of northwestern Tianshan. Similarly, Wang et al., (2007a) and Long et al., (2008) demonstrated that Carboniferous volcanic rocks of the same area belong to the calc-alkalic series, and have geochemical characteristics of arc volcanic rocks. The Dabate dacites (316 ± 6 Ma) also show a typical arc-like geochemical nature (Figs. 4d and 7a-b). We thus conclude that both the Late Carboniferous volcanic and plutonic rocks and the coeval Mo mineralization in northwestern Tianshan were related to the southward subduction of the Junggar Ocean beneath the YCTP.

5.4.4. 300-280 Ma (Fig. 13d)

Our new data for the Early Permian (289 ± 3 Ma) Dabate A-type granite porphyries are consistent with the proposed Early Permian rocks more likely mark a post-collisional extension event (Fig. 16d). There is other evidence in support of this conclusion. (1) Several A-type granites with ages around 290 Ma have been found in southern Tianshan (Konopelko et al., 2007), implying that southern Tianshan had entered a post-collisional stage by the Early-Permian. (2) High-K granites on the southern slope of the Alataw Mountains, with zircon U-Pb ages of 298.4 ± 5.7 Ma and 292 ± 4.9 Ma have been interpreted to be post-collisional granitic rocks, based on geochronological data and field studies (Liu et al., 2005). Two-mica granites from the southern margin of the Alataw Mountains have a similar zircon U-Pb age (290 ± 7 Ma; Chen et al., 2007) and whole rock ^{40}Ar-^{39}Ar age (299 ± 6 Ma; Chen et al., 1994), interpreted as representing a product of post-collisional crustal anatexis. (3) Wang et al. (2009) suggested that 294-280 Ma high-K calc-alkaline granites in the Borohoro area were formed in a post-collisional setting. (4) The diabasic porphyry formed in a post-collisional setting in the Baiyanggou area near the Urumqi city yields a zircons U-Pb age of 289 ± 5 Ma (Shu et al., 2005). (5) Early Permian bimodal magmatism in the region (Che et al., 1994) probably represents the early products of extension following the collision between the Junggar plate and the YCTP, and was associated with emplacement of the post-collisional Dabate A-type granite porphyries. In addition, an Early Permian regional dextral faulting episode in the Tianshan range is considered to have resulted from late collisional strike-slip (Laurent-Charvet et al., 2002).

Two alternative geodynamic models may explain magmatism in post-collisional settings: (a) slab breakoff (Davies and von Blackenburg, 1995; Whalen et al., 2006) and (b) large-scale lithosphere delamination (e.g. Lustrino, 2005) or convective removal of the lithosphere (e.g. Houseman et al., 1981). These processes are capable of causing partial melting in various sources including the ascended asthenosphere, the enriched lithospheric mantle, and even the overlying crust. The second model requires the removal of dense lithospheric root and wholesale melting of the lower crust as hot asthenosphere was emplaced close to the Moho (Houseman et al., 1981; Lustrino, 2005). Thus, the models predict large diffuse, non-linear zones of magmatism within the affected area (e.g., Wu et al., 2003; Whalen et al., 2006, 2010; Zhang et al., 2007; Aydin et al., 2008; Zhao et al., 2009; Liu et al., 2010). In contrast, the slab break-off model predicts a relatively narrow, linear zone of magmatism aligned with a major lineament (Davies and von Blackenburg, 1995; Whalen et al., 2006, 2010; Oyhantçabal et al., 2007). The slab break-off mechanism is favoured because the resultant narrow region of upwelling hot asthenosphere provides the appropriate thermal flux to melt overlying lower crust and generate the Permian A-type granitic rocks, which display a roughly linear distribution along the NTOB (Fig. 1; Fig. 13d). This inference is also supported by the presence of Early Permian mafic-ultramafic magmatic complexes along the NTOB (Zhou et al., 2004) that are coeval with the A-type granites and likely derived from asthenoshperic mantle sources (Whalen et al., 2006).

7. Conclusions

The Lamasu intrusion associated with Cu-Au deposits in the northwestern Tianshan area are calc-alkaline plagioclase granites and granodiorite porphyries. They exhibit geochemical and petrologic characteristics that are similar to adakites. In the Dabate area, dacites are also associated with Cu-Mo deposits, but the granite porphyries, which are barren of metal mineralization, exhibit the geochemical and petrologic characteristics of A_2-type granites.

New zircon U-Pb ages indicate that the Lamasu intrusive rocks were emplaced at 366 ± 3Ma, whereas the Dabate dacite and A-type granite were emplaced at 316 ± 4 Ma and 289 ± 3 Ma, respectively. Thus, the magmatic rocks in the Lamasu-Dabate area were mainly generated in Late Devonian-Early Permian.

The Lamasu intrusive rocks were most likely generated by partial melting of southward subducted Junggar oceanic crust during the Late Devonian, and subsequent melt-mantle interaction and AFC by basement rocks in a normal, steep, subduction setting. The Late Carboniferous Dabate dacites were generated by melting of juvenile basaltic lower crust. A magmatic gap or quiescent period that existed between ca. 345 and 320 Ma is interpreted as a “flat-subduction” episode, which was likely followed by roll-back of the slab to steeper angles in a return to normal slab subduction during the Late Carboniferous. Therefore, the Late Devonian to Late Carboniferous volcanic and plutonic rocks in northwestern Tianshan constitute a typical calc-alkaline arc assemblage formed at an active continental margin as a result of southward subduction of the Junggar Ocean.

The Early Permian Dabate A-type granite porphyries were generated by partial melting of late Carboniferous igneous rocks by upwelling of hot asthenospheric mantle because of slab break-off during a post-collisional stage. Such Early Permian A-type granites mark the start of an extensional tectonic regime after the closure of the Junggar Ocean by the end of the Carboniferous.

Acknowledgements

We sincerely thank Professor Nelson Eby and two anonymous reviewers for their constructive and helpful reviews. We appreciate the assistance of Professors Liu Yongsheng and Yang Jinhui, and Ms./Mr. Yang Yueheng, Xie Liewei, Chen Haihong, Liu Ying, Hu Guangqian, Ma Jinlong, Liang Xirong and Tu Xianglin for geochronological and geochemical analyses. This study was jointly supported by the Major State Basic Research Program (973 Program) of People's Republic of China (No. 2007CB411308), the National Natural Science Foundation of China (Grant No. 40721063), the Knowledge Innovation Program of Chinese Academy of Sciences (KZCX2-YW-128), and the Institute for Geoscience Research (TIGeR) at Curtin University of Technology. This is contribution No. IS-XXXX from GIGCAS.

APPENDIX A. SUPPLEMENTARY DATA

Supplementary data associated with this article can be found, in the online version, at XXXXXX.

References

Allen, M.B., Sengor, A.M.C., Natal'in, B.A., 1995. Junggar, Turfan and Alakol basins as Late Permian to? Early Triassic extensional structures in a sinistral shear zone in the Altaid Orogenic Collage, Central Asia. Journal of the Geological Society 152(2), 327-338.

Allen, M.B., Windley, B.F., Zhang, C., 1993. Palaeozoic collisional tectonics and magmatism of the Chinese Tien Shan, central Asia. Tectonophysics 220(1-4), 89-115.

Atherton, M.P., Petford, N., 1993. Generation of sodium-rich magmas from newly underplated basaltic crust. Nature 362(6416), 144-146.

Aydin, F., Karsli, O., Chen, B., 2008. Petrogenesis of the Neogene alkaline volcanics with implications for post-collisional lithospheric thinning of the Eastern Pontides, NE Turkey. Lithos 104(1-4), 249-266.

Barbarin, B., 1999. A review of the relationships between granitoid types, their origins and their geodynamic environments. Lithos 46(3), 605-626.

Barth, A.P., Wooden, J.L., Tosdal, R.M., Morrison, J., 1995. Crustal contamination in the petrogenesis of a calc-alkalic rock series: Josephine Mountain intrusion, California. Geological Society of America Bulletin 107(2), 201-212.

Belousova, E.A., Griffin, W.L., Suzanne, Y.O.R., Fisher, N.I., 2002. Igneous zircon: Trace element composition as an indicator of source rock type. Contributions to Mineralogy and Petrology 143 (5), 602-622.

Bonin, B., 2007. A-type granites and related rocks: Evolution of a concept, problems and prospects. Lithos 97(1-2), 1-29.

Booker, J.R., Favetto, A., Pomposiello, M.C., 2004. Low electrical resistivity associated with plunging of the Nazca flat slab beneath Argentina. Nature 429(6990), 399-403.

Borg, L.E., Clynne, M.A., 1998. The Petrogenesis of Felsic Calc-alkaline Magmas from the Southernmost Cascades, California: Origin by Partial Melting of Basaltic Lower Crust. Journal of Petrology 39(6), 1197-1222.

Carroll, A.R., Graham, S.A., Hendrix, M.S., Ying, D., Zhou, D., 1995. Late Paleozoic tectonic amalgamation of northwestern China; sedimentary record of the northern Tarim, northwestern Turpan, and southern Junggar basins. Geological Society of America Bulletin 107(5), 571-594.

Castillo, P.R., Janney, P.E., Solidum, R.U., 1999. Petrology and geochemistry of Camiguin Island, southern Philippines: insights to the source of adakites and other lavas in a complex arc setting. Contributions to Mineralogy and Petrology 134(1), 33-51.

Che, Z.L., Liu, H.F., Liu, L., 1994. Forming and evolution of the Middle Tianshan. The Geological Publishing House Beijing, 135 pp (in Chinese with English abstract).

Chen, B.H., Luo, Z.H., Jia, B.H., Liu, W., W ei, Y., Han, Y.G., 2007. SHRIMP U-Pb zircon geochronology of igneous rocks from southern margin of the Alataw Mountains, Xinjiang, China. Acta Petrologica Sinica 23(7), 1756-1764 (in Chinese with English abstract).

Chen, L., Ma, C.Q., She, Z.B., Mason, R., Zhang, J.Y., Zhang, C., 2009. Petrogenesis and tectonic implications of A-type granites in the Dabie orogenic belt, China: geochronological and geochemical constraints. Geological Magazine 146(5), 638-651

Chen, J.F., Chen, D.G., Li, X.M., Zhou, T.X., Foland, K.A., 1994. K-Ar and $^{40}Ar/^{39}Ar$ geochronology of granites from the Alataw Mountains, northwest Xinjiang, China. Acta Petrologica Sinica 10(2), 184-192 (in Chinese with English abstract).

Chung, S.L., Liu, D.Y., Ji, J.Q., Chu, M.F., Lee, H.Y., Wen, D.J., Lo, C.H., Lee, T.Y., Qian, Q., Zhang, Q., 2003. Adakites from continental collision zones: Melting of thickened lower crust beneath southern Tibet. Geology 31(11), 1021-1024.

Chung, S.L., Chu, M.F., Zhang, Y.Q., Xie, Y.W., Lo, C.H., Lee, T.Y., Lan, C.Y., Li, X.H., Zhang, Q., Wang, Y.Z., 2005. Tibetan tectonic evolution inferred from spatial and temporal variations in post-collisional magmatism. Earth-Science Reviews 68(3-4), 173-196.

Coleman, R.G., 1989. Continental growth of Northwest China. Tectonics 8(3), 621-635.

Collins, W., Beams, S., White, A., Chappell, B., 1982. Nature and origin of A-type granites with particular reference to southeastern Australia. Contributions to Mineralogy and Petrology 80(2), 189-200.

Condie, K.C., 2005. TTGs and adakites: are they both slab melts? Lithos 80(1-4), 33-44.

Davies, J.H., von Blanckenburg, F., 1995. Slab breakoff: A model of lithosphere detachment and its test in the magmatism and deformation of collisional orogens. Earth and Planetary Science Letters 129(1-4), 85-102.

Defant, M.J., Drummond, M.S., 1990. Derivation of some modern arc magmas by melting of young subducted lithosphere. Nature 347(6294), 662-665.

Defant, M.J., Kepezhinskas, P., 2001. Adakites: A review of slab melting over the past decade and the case for a slab-melt component in arcs. EOS 82, 65-69

Defant, M.J., Kepezhinskas, P., Defant, M.J., Xu, J.F., Kepezhinskas, P., Wang, Q., Zhang, Q. and Xiao, L., 2002. Adakites: some variations on a theme. Acta Petrologica Sinica 18(2), 129-142.

Ding, L., Kapp, P., Zhong, D.L., Deng, W.M., 2003. Cenozoic Volcanism in Tibet: Evidence for a Transition from Oceanic to Continental Subduction. Journal of Petrology 44(10), 1833-1865.

Ding, X., Lundstrom, C., Huang, F., Li, J., Zhang, Z.M., Sun, X.M., Liang, J.L. and Sun, W.D., 2009. Natural and experimental constraints on formation of the continental crust based on niobium-tantalum fractionation: International Geology Review 51(6), 473-501.

Eby, G.N., 1990. The A-type granitoids: A review of their occurrence and chemical characteristics and speculations on their petrogenesis. Lithos 26(1-2), 115-134.

Eby, G.N., 1992. Chemical subdivision of the A-type granitoids: petrogenetic and tectonic implications. Geology 20(7), 641-644.

Foley, S., Tiepolo, M., Vannucci, R., 2002. Growth of early continental crust controlled by melting of amphibolite in subduction zones. Nature 417(6891), 837-840.

Förster, H.J., Tischendorf, G., Trumbull, R.B., 1997. An evaluation of the Rb vs. (Y + Nb) discrimination diagram to infer tectonic setting of silicic igneous rocks. Lithos 40(2-4), 261-293.

Frost, B.R., Barnes, C.G., Collins, W.J., Arculus, R.J., Ellis, D.J., Frost, C.D., 2001. A Geochemical Classification for Granitic Rocks. Journal of Petrology 42(11), 2033-2048.

Gao, J., Li, M.S., Xiao, X.C., Tang, Y.Q., He, G.Q., 1998. Paleozoic tectonic evolution of the Tianshan Orogen, northwestern China. Tectonophysics 287(1-4), 213-231.

Gao, S., Rudnick, R.L., Yuan, H.L., Liu, X.M., Liu, Y.S., Xu, W.L., Ling, W.L., Ayers, J., Wang, X.C., Wang, Q.H., 2004. Recycling lower continental crust in the North China Craton. Nature 432(7019), 892-897.

Geng, H., Sun, M., Yuan, C., Xiao, W., Xian, W., Zhao, G., Zhang, L., Wong, K., Wu, F., 2009. Geochemical, Sr-Nd and zircon U-Pb-Hf isotopic studies of Late Carboniferous magmatism in the West Junggar, Xinjiang: Implications for ridge subduction? Chemical Geology 266(3-4), 364-389.

Golovanov, I.M., Seltmann, R., Kremenetsky, A.A., 2005. The porphyry Cu-Au/Mo deposits of Central Eurasia 2. The Almalyk (kal'makyr-dalnee) and saukbulak Cu-Au porphyry systems, Uzbekistan. In: T.M. Porter (Editor), Super Porphyry Copper & Gold Deposits. PGC Publishing, Adelaide, Australia, pp. 513-523.

Griffin, W.L., Pearson, N.J., Belousova, E., Jackson, S.E., van Achterbergh, E., O'Reilly, S.Y., Shee, S.R., 2000. The Hf isotope composition of cratonic mantle: LAM-MC-ICPMS analysis of zircon megacrysts in kimberlites. Geochimica et Cosmochimica Acta 64(1), 133-147.

Guan. M.Z., Zeng, X.R., Dai, Y.L, Wei, J.T., Wang, H., Duan, S.Z., Zhu, Y., 1990. Comprehensive studies of geology, geochemistry and geophysics and targets selection in Lamasu Copper-polymetallic region. National 305 Project Items (No.4-7) (In Chinese).

Guo, Z., Wilson, M., Liu, J., 2007. Post-collisional adakites in south Tibet: Products of partial melting of subduction-modified lower crust. Lithos 96(1-2), 205-224.

Han, B.F., Guo, Z.J., Zhang, Z.C., Zheng, L., Chen, J.F., Song, B., 2010. Age, geochemistry, and tectonic implications of a late Paleozoic stitching pluton in the North Tian Shan suture zone, western China. Geological Society of America Bulletin 122(3-4), 627-640.

Houseman, G.A., McKenzie, D.P., Molnar, P., 1981. Convective instability of a thickened boundary layer and its relevance for the thermal evolution of continental convergent belts. Journal of Geophysical Research 86, 6115–6132.

Hu, A.Q., Jahn, B.M., Zhang, G.X., Chen, Y.B., Zhang, Q.F., 2000. Crustal evolution and Phanerozoic crustal growth in northern Xinjiang: Nd isotopic evidence. Part I. Isotopic characterization of basement rocks. Tectonophysics 328(1-2), 15-51.

Hu, A.Q., Wei, G.J., Zhang, J.B., Deng, W.F., Chen, L.L., 2008. SHRIMP U-Pb ages for zircons of the amphibolites and tectonic evolution significance from the Wenquan domain in the West Tianshan Mountains, Xinjiang, China. Acta Petrologica Sinica 24(12), 2731-2740 (in Chinese with English abstract).

Irvine, T.N., Baragar, W.R.A., 1971. A Guide to the Chemical Classification of the Common Volcanic Rocks. Canadian Journal of Earth Sciences 8(5), 523-548.

Kay, R.W., 1978. Aleutian magnesian andesites: Melts from subducted Pacific ocean crust. Journal of Volcanology and Geothermal Research 4(1-2), 117-132.

Kay, R.W., Kay, S.M., 1993. Delamination and delamination magmatism. Tectonophysics 219(1-3), 177-189.

Kay, S.M., Mpodozis, C., 2001. Central Andean Ore Deposits Linked to Evolving Shallow Subduction Systems and Thickening Crust. GSA Today 11(3), 4-9.

Kay, S.M., Ramos, V.A., Marquez, M., 1993. Evidence in Cerro Pampa volcanic rocks for slab-melting prior to ridge-trench collision in southern South America. Journal of Geology 101, 703-714.

Kerr, A., Fryer, B.J., 1993. Nd isotope evidence for crust-mantle interaction in the generation of A-type granitoid suites in Labrador, Canada. Chemical Geology 104(1-4): 39-60.

King, P.L., White, A.J.R., Chappell, B.W., Allen, C.M., 1997. Characterization and origin of aluminous A-type granites from the Lachlan Fold Belt, Southeastern Australia. Journal of Petrology 38(3), 371-391.

Konopelko, D., Biske, G., Seltmann, R., Eklund, O., Belyatsky, B., 2007. Hercynian post-collisional A-type granites of the Kokshaal Range, Southern Tien Shan, Kyrgyzstan. Lithos 97(1-2), 140-160.

Kröner, A., Hegner, E., Lehmann, B., Heinhorst, J., Wingate, M.T.D., Liu, D.Y., Ermelov, P., 2008. Palaeozoic arc magmatism in the Central Asian Orogenic Belt of Kazakhstan: SHRIMP zircon ages and whole-rock Nd isotopic systematics. Journal of Asian Earth Sciences 32(2-4), 118-130.

Laurent-Charvet, S., Charvet, J., Shu, L., Ma, R., Lu, H., 2002. Palaeozoic late collisional strike-slip deformations in Tianshan and Altay, Eastern Xinjiang, NW China. Terra Nova 14(4), 249-256.

Lee, H.-Y., Chung, S.-L., Lo, C.-H., Ji, J., Lee, T.-Y., Qian, Q., Zhang, Q., 2009. Eocene Neotethyan slab breakoff in southern Tibet inferred from the Linzizong volcanic record. Tectonophysics 477, 20-35.

Liang, J.L., Ding, X., Sun, X.M., Zhang, Z.M., Zhang, H., Sun, W.D., 2009. Nb/Ta fractionation observed in eclogites from the Chinese Continental Scientific Drilling Project: Chemical Geology 268, 27-40.

Liégeois, J.P., Navez, J., Hertogen, J., Black, R., 1998. Contrasting origin of post-collisional high-K calc-alkaline and shoshonitic versus alkaline and peralkaline granitoids. The use of sliding normalization. Lithos 45(1-4), 1-28.

Li, H.Q., Wang, D.H., Wan, Y., Qu, W.J., Zhang, B., Lu, Y.F., Mei, Y.P., Zou, S.L., 2006. Isotopic geochronology study and its significance of the Lailisigao'er Mo deposit, Xinjiang. Acta Petrologica Sinica 22(1005), 2437-2443 (in Chinese with English abstract).

Liu, D.Q., Chen, Y.C., Wang, D.H., Tang, Y.L., Zhou, R.H., Wang, J.L., Li, H.Q., Chen, F.W., 2003. A Discussion on Problems Related to Mineralization of Tuwu-Yandong Cu-Mo orefield in Hami, Xinjiang. Mineral Deposits 22(4), 334-344 (in Chinese with English abstract).

Liu, S., Hu, R., Gao, S., Feng, C., Feng, G., Coulson, I.M., Li, C., Wang, T., Qi, Y., 2010. Zircon U-Pb age and Sr-Nd-Hf isotope geochemistry of Permian granodiorite and associated gabbro in the Songliao Block, NE China and implications for growth of juvenile crust. Lithos 114(3-4), 423-436.

Liu, W., Fei, P.X., 2006. Methane-rich fluid inclusions from ophiolitic dunite and post-collisional mafic-ultramafic intrusion: The mantle dynamics underneath the Palaeo-Asian Ocean through to the post-collisional period. Earth and Planetary Science Letters 242(3-4), 286-301.

Liu, Z.Q., Han, B.F., Ji, J.Q., Li, Z.H., 2005. Ages and geochemistry of the post-collisional granitic rocks from Eastern Alataw Mountains, Xinjiang, and implications for vertical crustal growth. Acta Petrologica Sinica 21(3), 623-639 (in Chinese with English abstract).

Long, L.L., Gao, J., Qian, Q., Xiong, X.M., Wang, J.B., Wang, Y.W., Gao, L.M., 2008. Geochemical charactersitics and tectonic setting of Carboniferous volcanic rocks form Yili region, western Tianshan. Acta Petrologica Sinica 24(4), 0699-710 (in Chinese with English abstract).

Lustrino, M., 2005. How the delamination and detachment of lower crust can influence basaltic magmatism. Earth-Science Reviews 72(1-2), 21-38.

Ma, C., Li, Z., Ehlers, C., Yang, K., Renjing, W., 1998. A post-collisional magmatic plumbing system: Mesozoic granitoid plutons from the Dabieshan high-pressure and ultrahigh-pressure metamorphic zone, east-central China. Lithos 45(1-4), 431-456.

Macpherson, C.G., Dreher, S.T., Thirlwall, M.F., 2006. Adakites without slab melting: High pressure differentiation of island arc magma, Mindanao, the Philippines. Earth and Planetary Science Letters 243(3-4), 581-593.

Martin, H., Smithies, R.H., Rapp, R., Moyen, J.F., Champion, D., 2005. An overview of adakite, tonalite-trondhjemite-granodiorite (TTG), and sanukitoid: relationships and some implications for crustal evolution. Lithos 79(1-2), 1-24.

Massimo, C., Dmitry, K., Reimar, S., Robert, A.C., 2006. Lead isotope variations across terrane boundaries of the Tien Shan and Chinese Altay. Mineralium Deposita 41(5), 411-428.

McKenzie, D., O'Nions, R.K., 1991. Partial Melt Distributions from Inversion of Rare Earth Element Concentrations. Journal of Petrology 32(5), 1021-1091.

Moyen, J.-F., Stevens, G., 2006. Experimental constraints on TTG petrogenesis: implications for Archean geodynamics. in Archean geodynamics and environments. K. Benn, J.-C. Mareschal and K. C. Condie, Eds., AGU.monographs 164, 149-178.

Muir, R.J., Weaver, S.D., Bradshaw, J.D., Eby, G.N., Evans, J.A., 1995. The Cretaceous Separation Point batholith, New Zealand: granitoid magmas formed by melting of mafic lithosphere. Journal of the Geological Society 152(4), 689-701.

Mungall, J.E., 2002. Roasting the mantle: Slab melting and the genesis of major Au and Au-rich Cu deposits. Geology 30(10), 915-918.

Oyhantçabal, P., Siegesmund, S., Wemmer, K., Frei, R., Layer, P., 2007. Post-collisional transition from calc-alkaline to alkaline magmatism during transcurrent deformation in the southernmost Dom Feliciano Belt (Braziliano-Pan-African, Uruguay). Lithos 98(1-4), 141-159.

Pearce, J.A., Harris, N.B.W., Tindle, A.G., 1984. Trace Element Discrimination Diagrams for the Tectonic Interpretation of Granitic Rocks. Journal of Petrology 25(4): 956-983.

Peccerillo, A., Taylor, S.R., 1976. Geochemistry of Eocene calc-alkaline volcanic rocks from the Kastamonu area, Northern Turkey. Contributions to Mineralogy and Petrology 58(1), 63-81.

Pirajno, F., Mao, J.W., Zhang, Z.C., Zhang, Z.H., Chai, F.M., 2008. The association of mafic-ultramafic intrusions and A-type magmatism in the Tian Shan and Altay orogens, NW China: Implications for geodynamic evolution and potential for the discovery of new ore deposits. Journal of Asian Earth Sciences 32(2-4), 165-183.

Qin, K., Sun, S., Li, J., Fang, T., Wang, S., Liu, W., 2002. Paleozoic Epithermal Au and Porphyry Cu Deposits in North Xinjiang, China: Epochs, Features, Tectonic Linkage and Exploration Significance. Resource Geology 52(4), 291-300.

Ramos, V.A., Folguera, A., 2009. Andean flat-slab subduction through time. Geological Society, London, Special Publication 327(1), 31-54.

Rapp, R.P., Shimizu, N., Norman, M.D., Applegate, G.S., 1999. Reaction between slab-derived melts and peridotite in the mantle wedge: experimental constraints at 3.8 GPa. Chemical Geology 160(4), 335-356.

Rapp, R.P., Watson, E.B., 1995. Dehydration Melting of Metabasalt at 8-32 kbar: Implications for Continental Growth and Crust-Mantle Recycling. Journal of Petrology 36(4), 891-931.

Reich, M., Parada, M.A., Palacios, C., Dietrich, A., Schultz, F., Lehmann, B., 2003. Adakite-like signature of Late Miocene intrusions at the Los Pelambres giant porphyry copper deposit in the Andes of central Chile: metallogenic implications. Mineralium Deposita 38(7), 876-885.

Richards, J.P., Kerrich, R., 2007. Special Paper: Adakite-Like Rocks: Their Diverse Origins and Questionable Role in Metallogenesis. Economic Geology 102(4), 537-576.

Rivers, T., Corrigan, D., 2000. Convergent margin on southeastern Laurentia during the Mesoproterozoic: Tectonic implications. Canadian Journal of Earth Sciences 37(2-3), 359-383.

Seltmann, R., Porter, T.M., 20005. The porphyry Cu–Au/Mo deposits of Central Eurasia 1. Tectonic, geologic and metallogenic setting, and significant deposits. In: T.M. Porter (Editor), Super Porphyry Copper & Gold Deposits: A Global Perspective. PGC Publishing, Adelaide, Australia, pp 467-512.

Sen, C., Dunn, T., 1994. Dehydration melting of a basaltic composition amphibolite at 1.5 and 2.0 GPa: implications for the origin of adakites. Contributions to Mineralogy and Petrology 117(4), 394-409.

Sengör, A.M.C., Natal'in, B.A., Burtman, V.S., 1993. Evolution of the Altaid tectonic collage and Palaeozoic crustal growth in Eurasia. Nature 364(6435), 299-307.

Shu, L.S., Zhu, W.B., Wang, B., Faure, M., Charvet, J., Cluzel, D., 2005. The post-collision intracontinental rifting and olistostrome on the southern slope of Bogda Mountains, Xinjiang. Acta Petrologica Sinica 21(1), 25-36 (in Chinese with English abstract).

Stern, C.R., Kilian, R., 1996. Role of the subducted slab, mantle wedge and continental crust in the generation of adakites from the Andean Austral Volcanic Zone. Contributions to Mineralogy and Petrology 123(3), 263-281.

Streckeisen, A., Le Maitre, R.W., 1979. A chemical approximation to the modal QAPF classification of the igneous rocks. Neues Jahrbuch für Mineralogie, Abhandlungen 136, 169-206.

Sun, S.S., McDonough, W.F., 1989. Chemical and isotopic systematics of oceanic basalts: implications for mantle composition and processes. Geological Society London Special Publications 42(1), 313–345.

Tang, G.J., Wang, Q., Zhao, Z.H., Wyman, D.A., Chen, H.H., Jiang, Z.Q., Jia, X.H., 2009. LA-ICP-MS zircon U-Pb Geochronology, element geochemistry and petrogenesis of the andesites in the gold-mineralization area of the eastern Taerbieke, western Tianshan. Acta Petrologica Sinica 025(06), 1341-1352 (in Chinese with English abstract).

Tatsumi, Y., Eggins, S., 1995. Subduction zone magmatism. Blackwell Publishing, Boston.

Turner, S.P., Foden, J.D., Morrison, R.S., 1992. Derivation of some A-type magmas by fractionation of basaltic magma: An example from the Padthaway Ridge, South Australia. Lithos 28(2), 151-179.

Wang, B., Cluzel, D., Shu, L., Faure, M., Charvet, J., Chen, Y., Meffre, S., de Jong, K., 2009. Evolution of calc-alkaline to alkaline magmatism through Carboniferous convergence to Permian transcurrent tectonics, western Chinese Tianshan. International Journal of Earth Sciences 98(6), 1275-1298.

Wang, B., Faure, M., Cluzel, D., Shu, L., Charvet, J., Meffre, S., Qian, M., 2006a. Late Paleozoic tectonic evolution of the northern West Chinese Tianshan Belt. Geodinamica Acta 19(3-4), 227-237.

Wang, B., Shu, L.S., Cluzel, D., Faure, M., Charvet, J., 2007a. Geochemical constraints on Carboniferous volcanic rocks of the Yili Block (Xinjiang, NW China): Implication for the tectonic evolution of Western Tianshan. Journal of Asian Earth Sciences 29(1), 148-159.

Wang, J.B., Xu, X., 2006. Post-collisional tectonic evolution and metallogenesis in Northern Xinjiang, China. Acta Geologica Sinica 80(1), 23-31(in Chinese with English Abstract).

Wang, Q., McDermott, F., Xu, J.F., Bellon, H., Zhu, Y.T., 2005. Cenozoic K-rich adakitic volcanic rocks in the Hohxil area, northern Tibet: Lower-crustal melting in an intracontinental setting. Geology 33(6), 465-468.

Wang, Q., Wyman, D.A., Xu, J., Jian, P., Zhao, Z., Li, C., Xu, W., Ma, J., He, B., 2007b. Early Cretaceous adakitic granites in the Northern Dabie Complex, central China: Implications for partial melting and delamination of thickened lower crust. Geochimica et Cosmochimica Acta 71(10), 2609-2636.

Wang, Q., Wyman, D.A., Zhao, Z.H., Xu, J.F., Bai, Z.H., Xiong, X.L., Dai, T.M., Li, C.F., Chu, Z.Y., 2007c. Petrogenesis of Carboniferous adakites and Nb-enriched arc basalts in the Alataw area, northern Tianshan Range (western China): Implications for Phanerozoic crustal growth in the Central Asia orogenic belt. Chemical Geology 236(1-2), 42-64.

Wang, Q., Xu, J.F., Jian, P., Bao, Z.W., Zhao, Z.H., Li, C.F., Xiong, X.L., Ma, J.L., 2006b. Petrogenesis of adakitic porphyries in an extensional tectonic setting, dexing, South China: Implications for the genesis of porphyry copper mineralization. Journal of Petrology 47(1), 119-144.

Wang, Q., Zhao, Z.H., Xu, J.F., Wyman, D.A., Xiong, X.L., Zi, F., Bai, Z.H., 2006c. Carboniferous adakite-high-Mg andesite-Nb-enriched basaltic rock suites in the Northern Tianshan area: Implications for Phanerozoic crustal growth in the Central Asia Orogenic Belt and Cu-Au mineralization. Acta Petrologica Sinica 22(1), 11-30 (in Chinese with English abstract).

Wen, D.R., Liu, D., Chung, S.L., Chu, M.F., Ji, J.Q., Zhang, Q., Song, B., Lee, T.Y., Yeh, M.W., Lo, C.H., 2008. Zircon SHRIMP U-Pb ages of the Gangdese Batholith and implications for Neotethyan subduction in southern Tibet. Chemical Geology 252(3-4), 191-201.

Whalen, J.B., Currie, K.L., Chappell, B.W., 1987. A-type granites: geochemical characteristics, discrimination and petrogenesis. Contributions to Mineralogy and Petrology 95(4), 407-419.

Whalen, J.B., McNicoll, V.J., van Staal, C.R., Lissenberg, C.J., Longstaffe, F.J., Jenner, G.A., van Breeman, O., 2006. Spatial, temporal and geochemical characteristics of Silurian collision-zone magmatism, Newfoundland Appalachians: An example of a rapidly evolving magmatic system related to slab break-off. Lithos 89(3-4), 377-404.

Whalen, J.B., Wodicka, N., Taylor, B.E., Jackson, G.D., 2010. Cumberland batholith, Trans-Hudson Orogen, Canada: Petrogenesis and implications for Paleoproterozoic crustal and orogenic processes. Lithos 117(1-4), 99-118.

Winchester, J.A., Floys, P.A., 1977. Geochemical discrimination of different magma series and their differentiation products using immobile elements. Chemical Geology 20, 325-343.

Windley, B.F., Allen, M.B., Zhang, C., Zhao, Z.Y., Wang, G.R., 1990. Paleozoic accretion and Cenozoic redeformation of the Chinese Tien Shan Range, Central Asia. Geology 18(2), 128-131.

Wu, F.Y., Jahn, B.M., Wilde, S.A., Lo, C.H., Yui, T.F., Lin, Q., Ge, W.C., Sun, D. Y., 2003. Highly fractionated I-type granites in NE China (II): Isotopic geochemistry and implications for crustal growth in the Phanerozoic. Lithos 67, 191-204.

Wu, F.Y., Sun, D.Y., Li, H.M., Jahn, B.M., Wilde, S., 2002. A-type granites in northeastern China: age and geochemical constraints on their petrogenesis. Chemical Geology 187(1-2), 143-173.

XBGMR (Xinjiang Bureau of Geology and Mineral Resources), 1993. Regional geology of Xinjiang Uygur Autonomy Region. Geology Publishing House, Beijing, pp 841.

Xia, L.Q., Xu, X.Y., Xia, Z.C., Li, X.M., Ma, Z.P., Wang, L.S., 2004a. Petrogenesis of Carboniferous rift-related volcanic rocks in the Tianshan, northwestern China. Geological Society of America Bulletin 116(3-4), 419-433.

Xia, L.Q., Xia, Z.C., Xu, X.Y., Li, X.M., Ma, Z.P., Wang, L.S., 2004b. Carboniferous Tianshan igneous megaprovince and mantle plume. Geologcal Bulletin of China 23(9), 903-910 (in Chinese with English abstract).

Xiao, L., Clemens, J.D., 2007. Origin of potassic (C-type) adakite magmas: Experimental and field constraints. Lithos 95(3-4), 399-414.

Xiao, L., Nick, H., Graham, B., Fu, M., Wang, F.Z., Franco, P., 2005. The Jinxi-Yelmand high-sulfidation epithermal gold deposit, Western Tianshan, Xinjiang Province, P.R. China. Ore Geology Reviews 26(1-2), 17-37.

Xiao, W.J., Han, C.M., Yuan, C., Sun, M., Lin, S.F., Chen, H.L., Li, Z.L., Li, J.L., Sun, S., 2008. Middle Cambrian to Permian subduction-related accretionary orogenesis of Northern Xinjiang, NW China: Implications for the tectonic evolution of central Asia. Journal of Asian Earth Sciences 32(2-4), 102-117.

Xiao, W.J., Windley, B.F., Yuan, C., Sun, M., Han, C.M., Lin, S.F., Chen, H.L., Yan, Q.R., Liu, D.Y., Qin, K.Z., Li, J.L., Sun, S., 2009. Paleozoic multiple subduction-accretion processes of the southern Altaids. American Journal of Science 309(3), 221-270.

Xiao, W.J., Zhang, L.C., Qin, K.Z., Sun, S., Li, J.L., 2004. Paleozoic accretionary and collisional tectonics of the eastern Tianshan (China): Implications for the continental growth of central Asia. American Journal of Science 304(4), 370-395.

Xiao, X.C., Tang, Y.Q., Li, J.Y., Zhao, M., Feng, Y.M., Zhu, B.Q., 1991. On tectonic evolution of the southern margin of the Paleozoic composite megasuture zone. In: X.C. Xiao and Y.Q. Tang (Editors), On Tectonic Evolution of the Southern Margin of the Paleozoic Composite Megasuture Zone. Beijing Technology Press, Beijing, pp. 1-29 (in Chinese).

Xiao, Y.L., Sun, W.D., Hoefs, J., Simon, K., Zhang, Z.M., Li, S.G., Hofmann, A.W., 2006, Making continental crust through slab melting: Constraints from niobium-tantalum fractionation in UHP metamorphic rutile: Geochimica Et Cosmochimica Acta 70, 4770-4782.

Xu, J.F., Shinjo, R., Defant, M.J., Wang, Q.A., Rapp, R.P., 2002. Origin of Mesozoic adakitic intrusive rocks in the Ningzhen area of east China: Partial melting of delaminated lower continental crust? Geology 30(12), 1111-1114.

Xu, X.Y., Li, X.M., Ma, Z.P., Xia, L.Q., Xia, Z.C., Peng, S.X., 2006a. LA-ICPMS Zircon U-Pb dating of gabbro from the Bayingou Ophiolite in the Northern Tianshan Mountains. Acta Geologica Sinica 80(8), 1168-1176 (in Chinese with English abstract).

Xu, X.Y., Ma, Z.P., Xia, Z.C., Xia, L.Q., Li, X.M., Wang, L.S., 2006b. TIMS U-Pb Isotopic Dating and Geochemical Characteristics of Paleozoic Granitic Rocks from the Middle-Western Section of Tianshan. Northwestern Geology 39(1), 50-75 (in Chinese with English abstract).

Yakubchuk, A., 2004. Architecture and mineral deposit settings of the Altaid orogenic collage: a revised model. Journal of Asian Earth Sciences 23(5), 761-779.

Yang, J.H., Wu, F.Y., Chung, S.L., Wilde, S.A., Chu, M.F., 2006. A hybrid origin for the Qianshan A-type granite, northeast China: Geochemical and Sr-Nd-Hf isotopic evidence. Lithos 89(1-2), 89-106.

Yin, J., Yuan, C., Sun, M., Long, X., Zhao, G., Wong, K.P., Geng, H., Cai, K., 2009. Late Carboniferous high-Mg dioritic dikes in Western Junggar, NW China: Geochemical features, petrogenesis and tectonic implications. Gondwana Research 17(1), 145-152.

Zhai, W., Sun, X.M., Gao, J., He, X.P., Liang, J.L., Miao, L.C., Wu, Y.L., 2006. SHRIMP dating of zircons from volcanic host rocks of Dahalajunshan Formation in Axi gold deposit, Xinjiang, China, and its geological implications. Acta Petrologica Sinica 22(5), 1399-1404 (in Chinese with English abstract).

Zhai, W., Sun, X.M., Sun, W.D., Su, L.W., He, X.P., Wu, Y.L., 2009. Geology, geochemistry, and genesis of Axi: A Paleozoic low-sulfidation type epithermal gold deposit in Xinjiang, China, Ore Geology Reviews 36(04), 265-281.

Zhang, D.Y., Zhang, Z.C., Ai, Y., Su, H.M., 2009. Geochronology, geochemistry of the Ores-Bearing Porphyries in the Lailisigao'er Region, Western Tianshan: implications for their tectonic setting and mineralization. Acta Petrologica Sinica 025(06), 1319-1331 (in Chinese with English abstract).

Zhang, H.F., Parrish, R., Zhang, L., Xu, W.C., Yuan, H.L., Gao, S., Crowley, Q.G., 2007. A-type granite and adakitic magmatism association in Songpan-Garze fold belt, eastern Tibetan Plateau: Implication for lithospheric delamination. Lithos 97(3-4), 323-335.

Zhang, L.C., Xiao, W.J., Qin, K.Z., Zhang, Q., 2006a. The adakite connection of the Tuwu-Yandong copper porphyry belt, eastern Tianshan, NW China: trace element and Sr-Nd-Pb isotope geochemistry. Mineralium Deposita 41(2), 188-200.

Zhang, Y.P., Wang, R., Wang, D.G., 2008a. Kekesai granite diorite-porphyry body zircon SHRIMP U-Pb dating and the prospecting significance in Bole city, Xinjiang. Xinjiang Geology 26(4), 340-342 (in Chinese with English abstract).

Zhang, Z.H., Mao, J.W., Wang, Z.L., Du, A.D., Wang, L.S., Wang, J.W., Qu.W.J, 2006b. Geology and metallogenetic epoch of the Dabate Porphyry Copper Deposit in West Tianshan Mountains, Xinjiang. Geological Review 52(5), 683-689 (in Chinese with English abstract).

Zhang, Z.H., Wang, Z.L., Du, A.D., Zuo, G.C., Liu, M., Wang, L.S., Wang, J.W., 2008b. Tectonic setting of the volcanic rocks in Dabate district and their Constraints on the ore-forming of porphyry ore, West Tianshan Mountains. Acta Geologica Sinica 82(11), 1494-1503 (in Chinese with English abstract).

Zhang, Z.H., Wang, Z.L., Wang, L.S., Zuo, G.C., 2008c. Metallogenic epoch and ore-forming environment of the Lamasu skarn-porphyritic Cu-Zn deposot, Western Tianshan, Xinjiang, NW China. Acta Geologica Sinica 82(4), 731-740 (in Chinese with English abstract).

Zhao, Z., Mo, X., Dilek, Y., Niu, Y., DePaolo, D.J., Robinson, P., Zhu, D., Sun, C., Dong, G., Zhou, S., Luo, Z., Hou, Z., 2009. Geochemical and Sr-Nd-Pb-O isotopic compositions of the post-collisional ultrapotassic magmatism in SW Tibet: Petrogenesis and implications for India intra-continental subduction beneath southern Tibet. Lithos 113(1-2), 190-212.

Zhou, M.F., Michael Lesher, C., Yang, Z.G., Li, J.W., Sun, M., 2004. Geochemistry and petrogenesis of 270 Ma Ni-Cu-(PGE) sulfide-bearing mafic intrusions in the Huangshan district, Eastern Xinjiang, Northwest China: implications for the tectonic evolution of the Central Asian orogenic belt. Chemical Geology 209(3-4), 233-257.

Zhu, Z.X., Wang, K.Z., Xu, D., Su, Y.L., Wu, Y.M., 2006. SHRIMP U-Pb dating of zircons from Carboniferous intrusive rocks on the active continental margin of Eren Habirga, West Tianshan, Xinjiang, China, and its geological implications. Geologcal Bulletin of China 25(8), 986-991(in Chinese with English abstract).

Figures

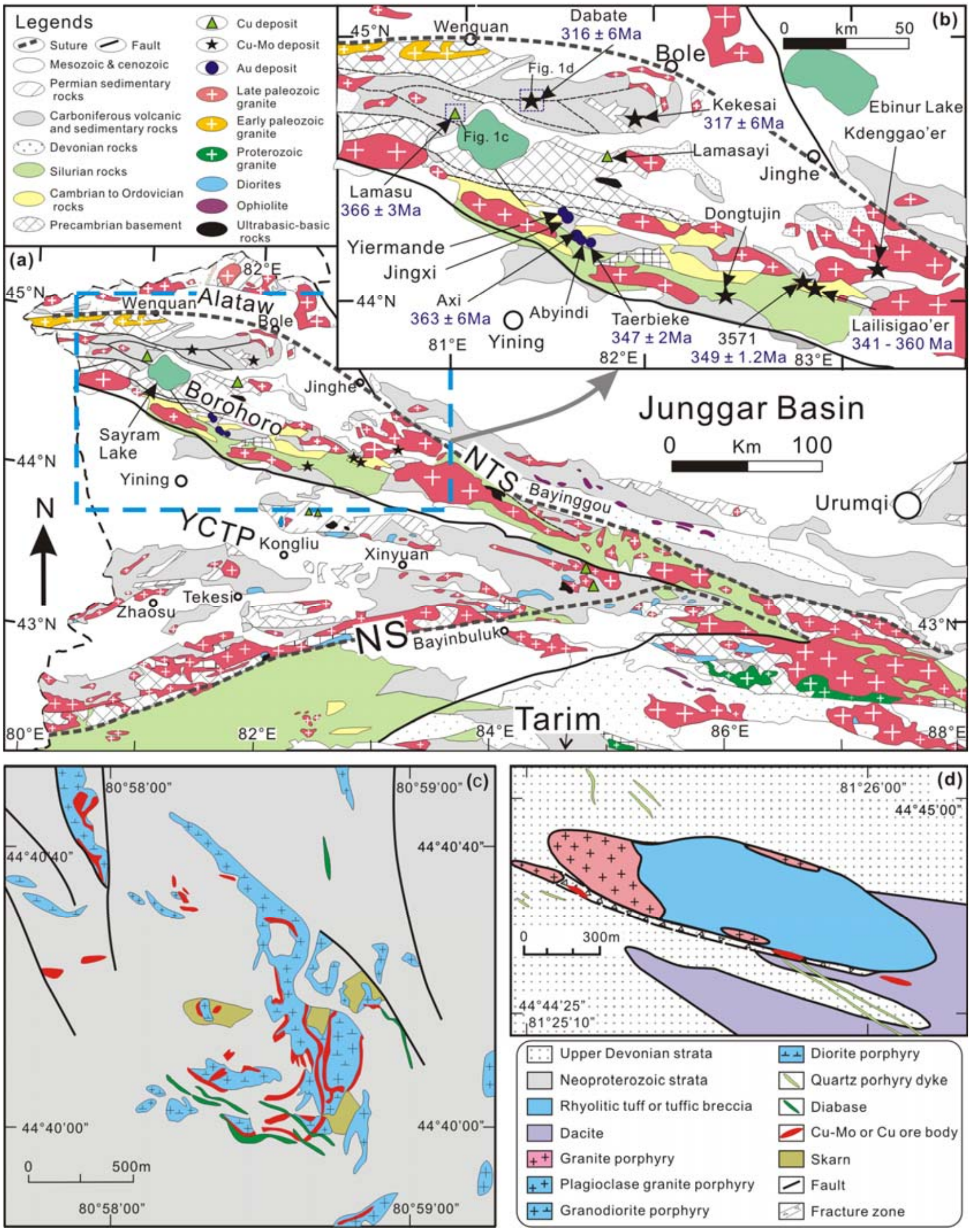

Fig. 1. Geological map of the northwestern Tianshan (west China) showing the location of porphyry copper and epithermal gold deposits (modified from Xinjiang Bureau of Geology and Mineral Resources (XBGMR, 1993). The age data for the Cu-Mo-Au deposits are from Li et al.

(2006), Zhai et al. (2006), Zhang et al. (2008b, 2009), Tang et al. (2009) and this study. YCTP-Yili-Central Tianshan plate. NTS-North Tianshan Suture: the boundary between the Junggar and Yili-Central Tianshan Plates; NS-Nalati Suture: the boundary between the Yili-Central Tianshan and Tarim plates.

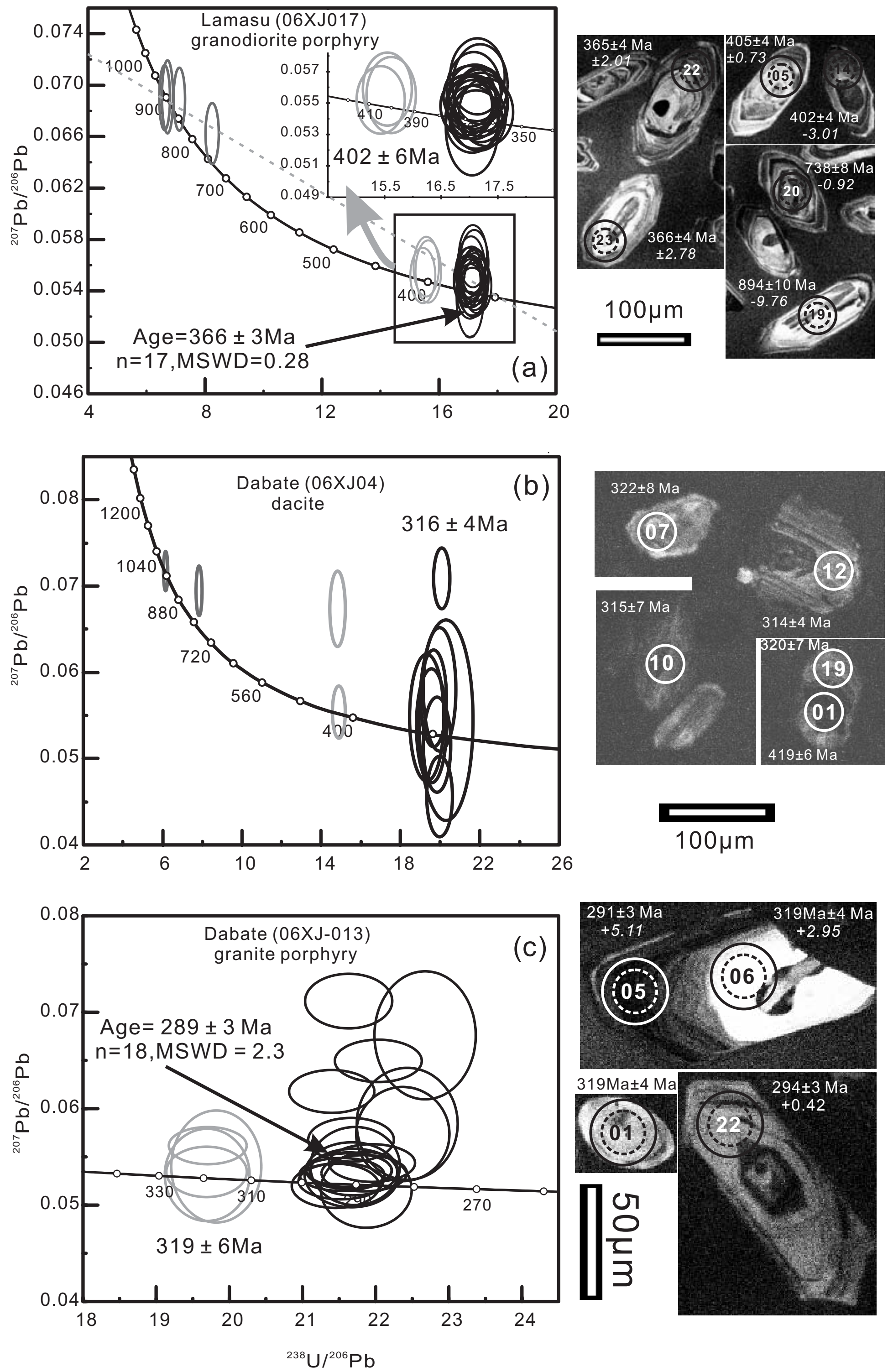

Fig. 2. LA-ICP-MS U-Pb zircon Tera-Wasserburg diagrams with cathodoluminescence images for (a) a granodiorite porphyry and a dacite and a granite porphyry (b-c) from the Lamasu and Dabate areas, respectively. Dashed and solid line circles indicate the locations of age and Hf

isotope analysis sites, respectively, with numbers in the circles representing spot numbers. The age and εHf(t) values for each spot are given.

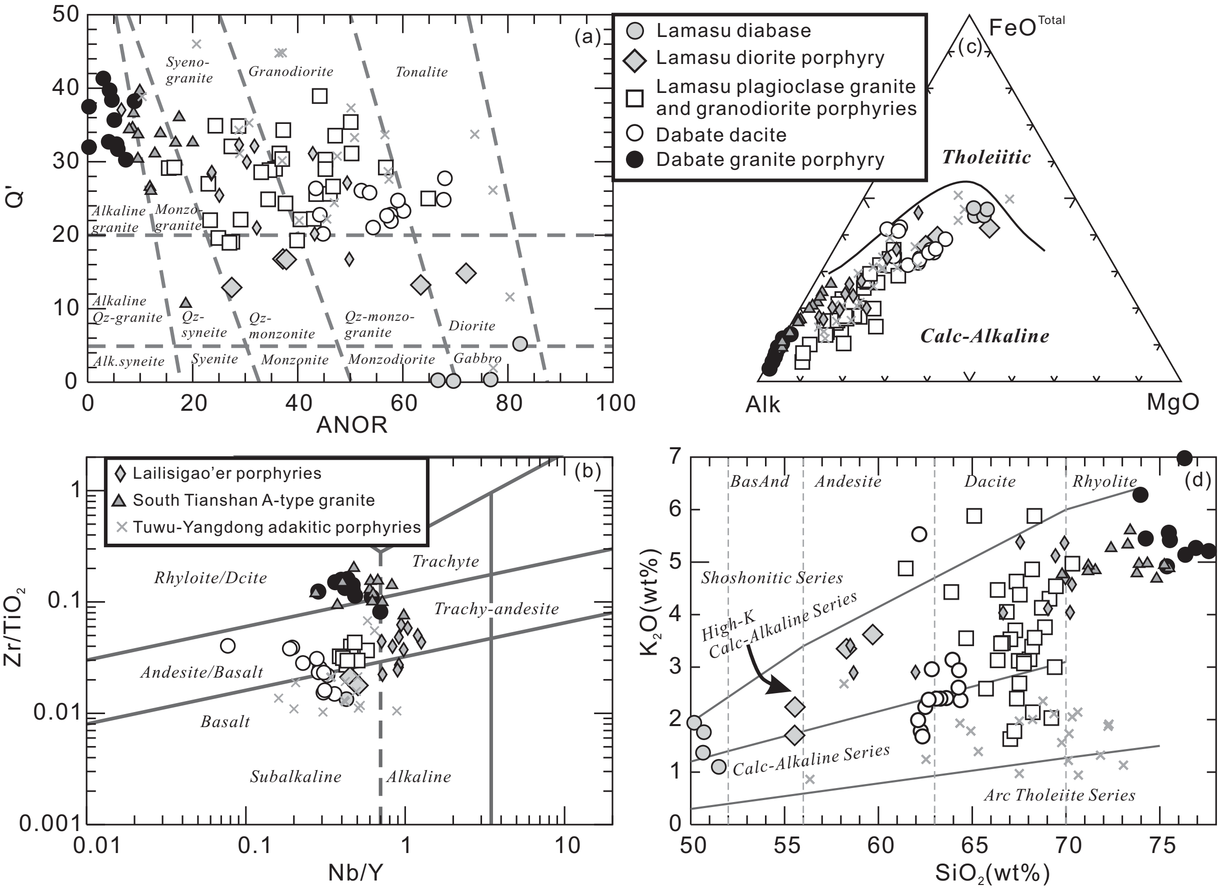

Fig. 3. (a) Q'-ANOR normative composition diagram (Streckeisen and Le Maitre, 1979). (b) Zr/TiO_2-Nb/Y discrimination diagram (Winchester and Floys, 1977). (c) AFM plot (Irvine and Baragar, 1971). (d) SiO_2 - K_2O plot (Peccerillo and Taylor, 1976). Data for the Lamasu samples are from Appendix 3 and Guan et al., (1990). Data for the Dabate samples are from Appendix 3 and Zhang et al., (2008b). Data for Lailisigao'er porphyries are from Zhang et al.,(2009). The south Tianshan A-type granites are from Konopelko et al.,(2007). The Tuwu-Yandong porphyries are from Zhang ea al., (2006a) and reference therein.

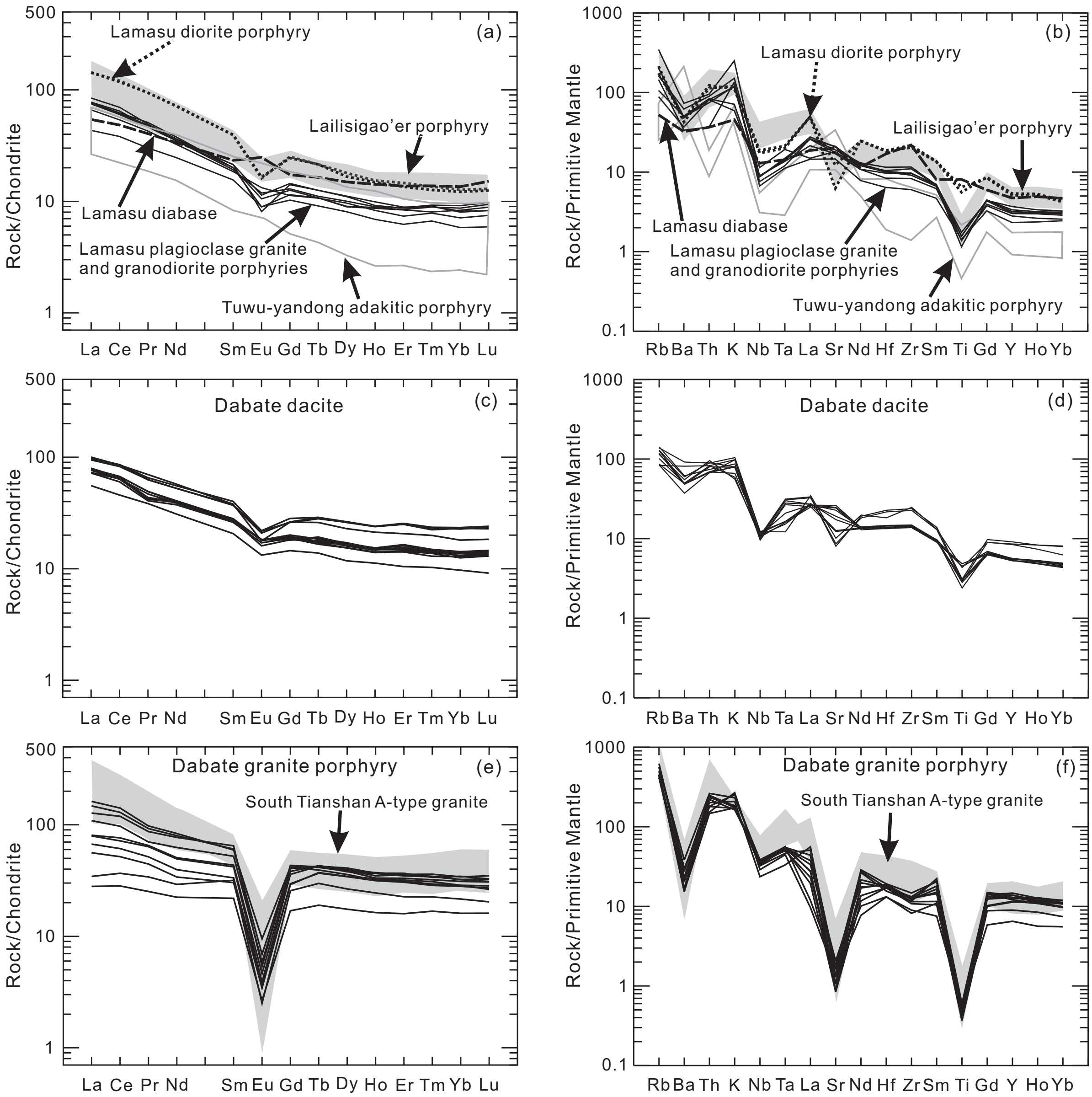

Fig. 4. Chondrite-normalized REE patterns (a, c, e) and primitive mantle normalized trace elements diagrams (b, d, f) for Lamasu and Dabate samples from the NTOB compared with the Lailisigao’er and Tuwu-Yandong porphyries and the South Tianshan A-type granites (Data sources as for Fig. 3). Chondrite and primitive mantle normalized values are from Sun and McDonough (1989).

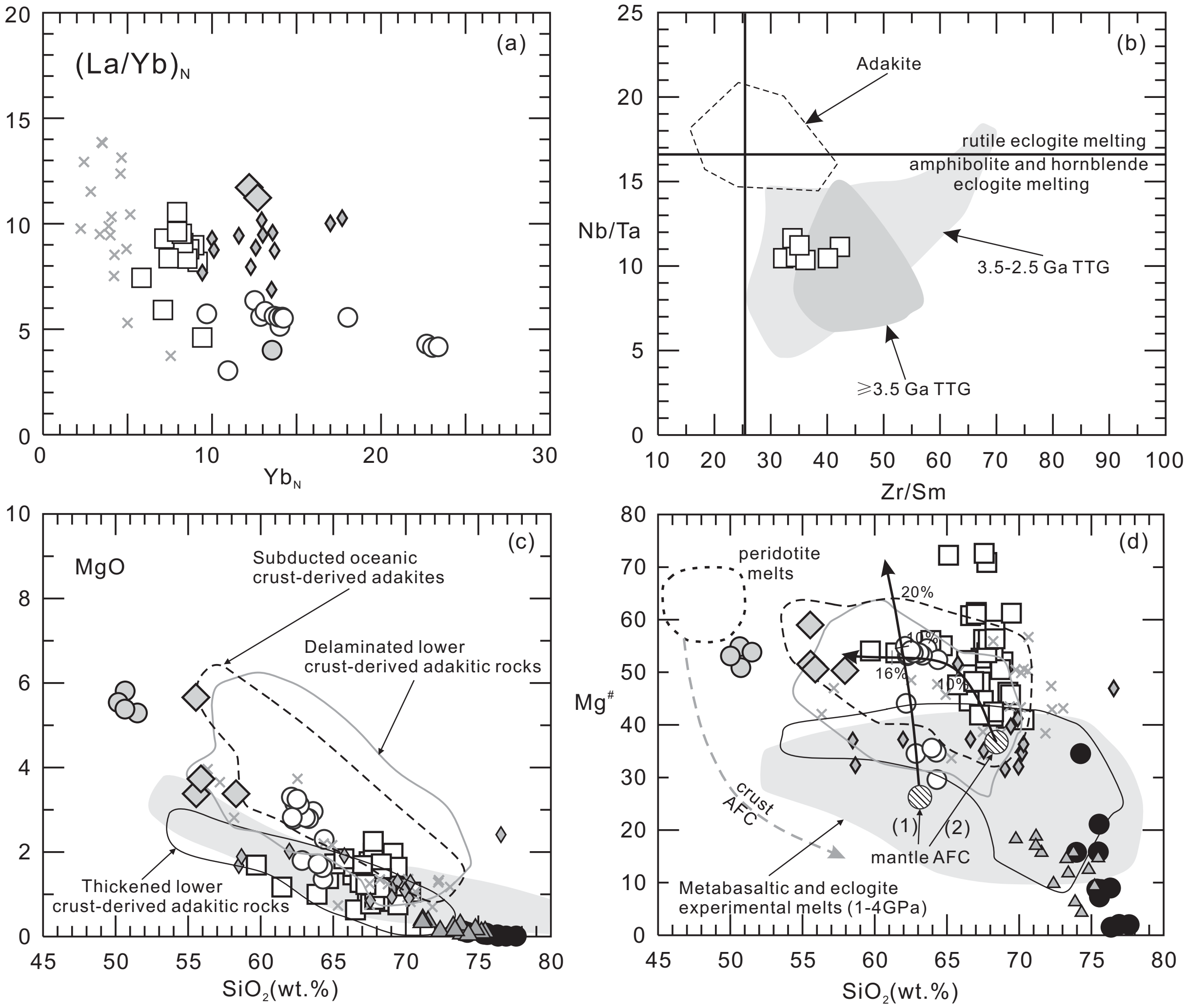

Fig. 5. (a) Yb_N versus $(La/Yb)_N$ diagram. (b) Nb/Ta versus Zr/Sm diagram (Foley et al., 2002). (c) SiO_2 versus MgO diagram. (d) SiO_2 versus $Mg^{\#}$ diagram. Mantle AFC curves, with proportions of assimilated peridotite indicated, are after Stern and Kilian (1996) (Curve 1) and Rapp et al., (1999) (Curve 2), peridotite melts and crust AFC curves from Stern and Kilian (1996). Data for metabasaltic and eclogite experimental melts (1-4.0 GPa), and peridotite-hybridized equivalents, are from Rapp et al., (1999) and references therein. The field for subducted oceanic crust-derived adakites, and delaminated or thickened lower crust-derived adakitic rocks after Wang et al. (2006). Data sources and symbols are same as in Fig. 3.

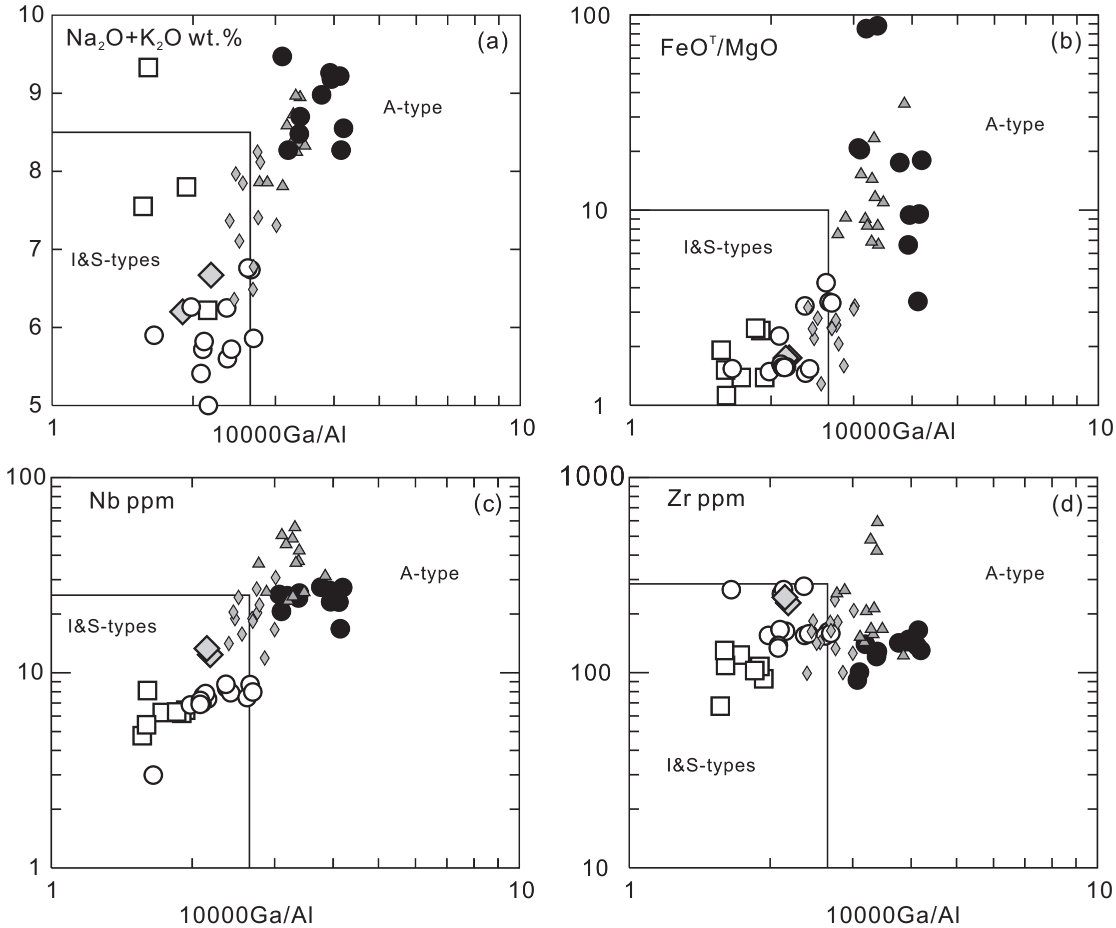

Fig. 6. Discrimination diagrams for A-type granites (Whalen et al., 1987). Dabate granitic porphyries plot in the field of A-type granite. Other magmatic rock samples are plotted for comparison. Data sources and symbols are the same as in Fig. 3.

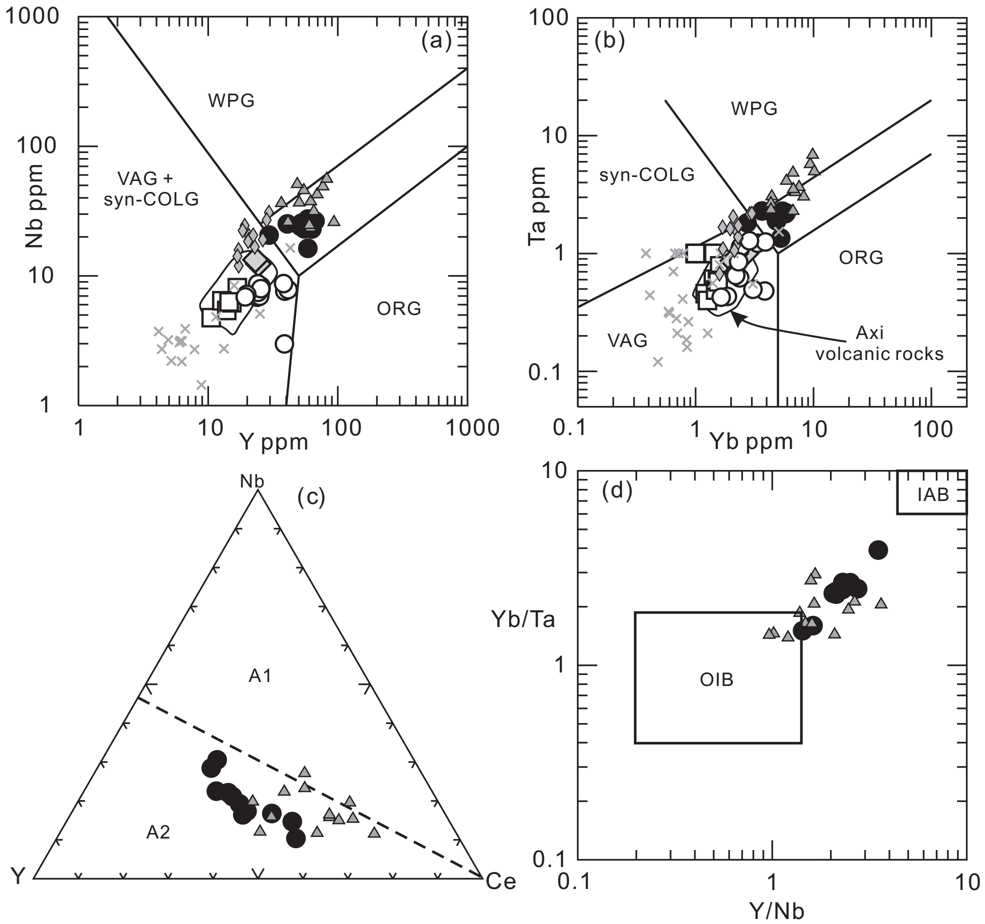

Fig. 7. Tectonic discrimination plot for granites (a and b) (Pearce et al., 1984). (c) A_1 and A_2 subgroup discrimination of A-type granites and (d) Y/Nb versus Yb/Ta diagram for Dabate granitic porphyry (Eby, 1992). Data sources and symbols are same as in Fig. 3.

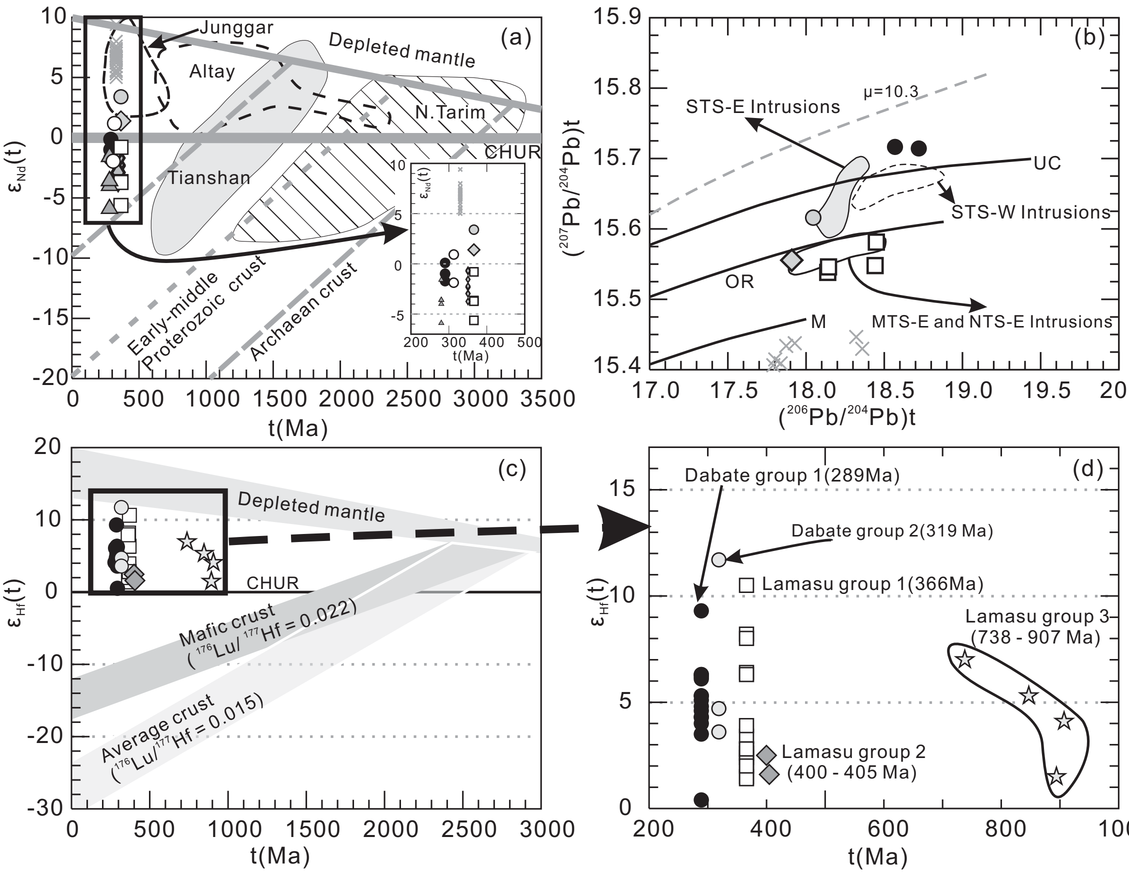

Fig. 8. $\varepsilon_{Nd}(t)$ and $\varepsilon_{Hf}(t)$ versus age diagram (a, c and d). Fields of basement rocks (amphibolites and gneisses) of the Junggar, Altay and Tianshan are from Hu et al. (2000). (b) $(^{206}Pb/^{204}Pb)_t$ versus $(^{207}Pb/^{204}Pb)_t$ diagram. Field of Tianshan (TS) intrusions are from Massimo et al. (2006). Data sources are from Appendix 4 and 5. Symbols are same as in Fig. 3.

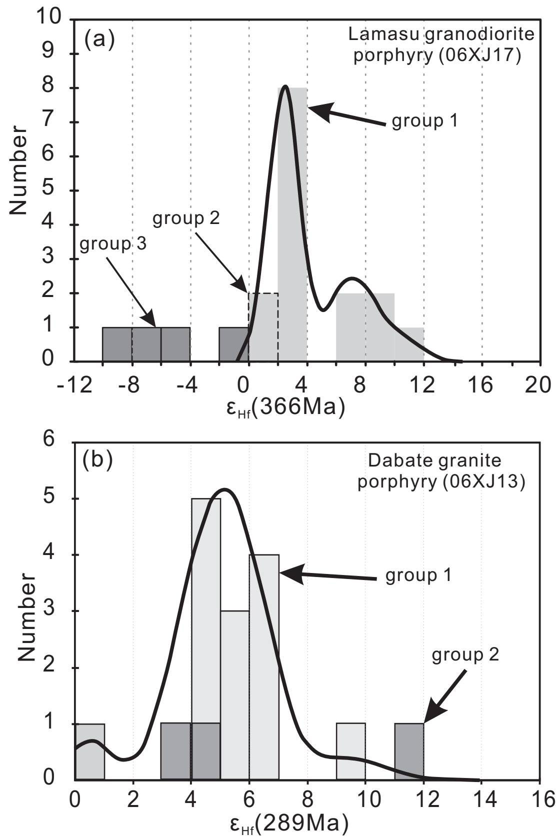

Fig. 9. Histogram of $\varepsilon_{Hf}(t)$ values for the Lamasu granodiorite porphyry (a) and the Dabate granite (b). Data sources are from Appendix 5.

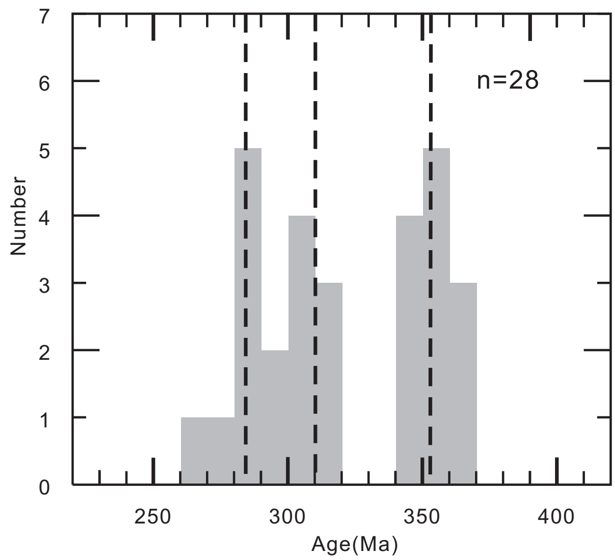

Fig. 10. Histograms of ages for the igneous rocks in the NTOB. Data sources: Li et al., 2006; Wang et al., 2009, 2007a, 2007c; Xu et al., 2006b; Zhai et al., 2006; Zhang et al., 2009, 2008a;,

2008b; Zhu et al., 2006 and this study.

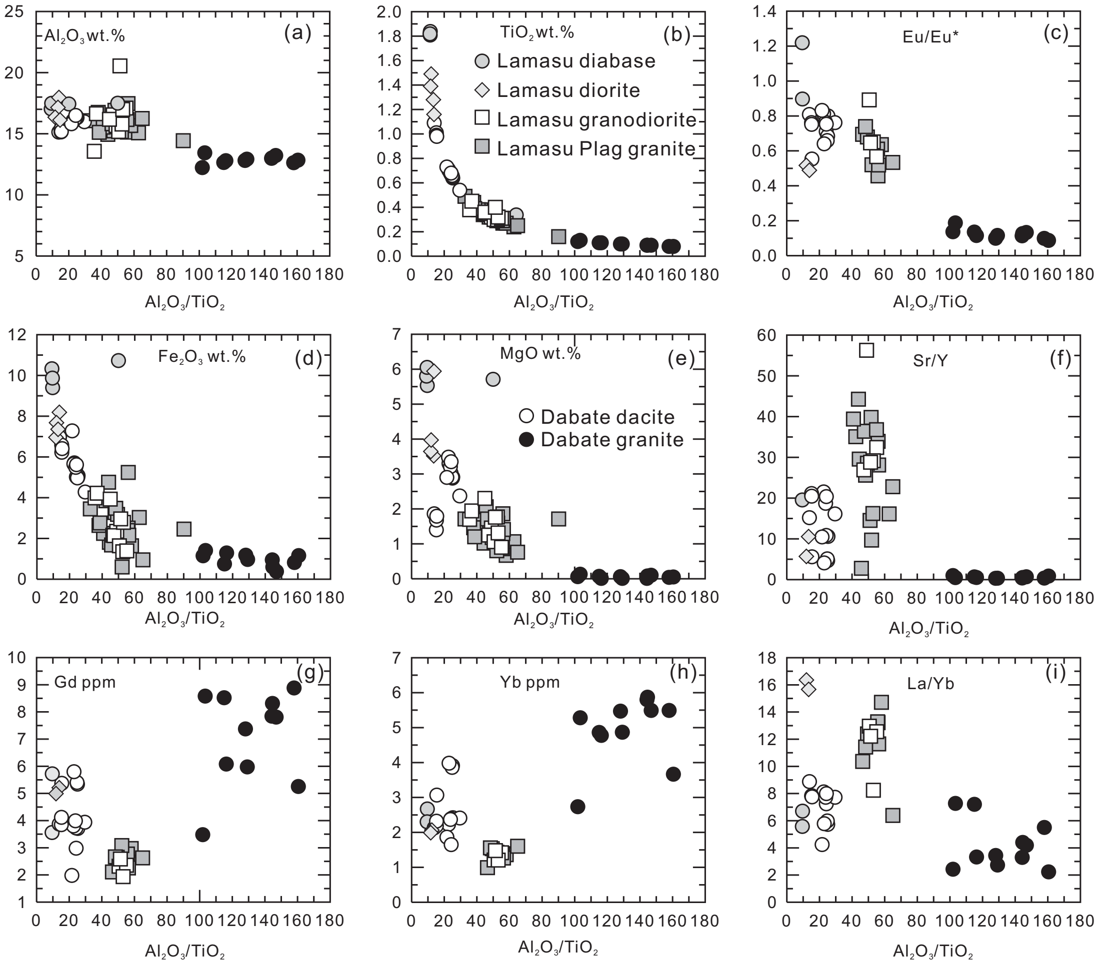

Fig. 11. Al_2O_3/TiO_2 versus Al_2O_3 (a), TiO_2 (b), Eu/Eu* (c), Fe_2O_3 (d), MgO (e), Yb (f), Gd (g), Sr/Y, and La/Yb (i). Data sources are same as in Fig. 3.

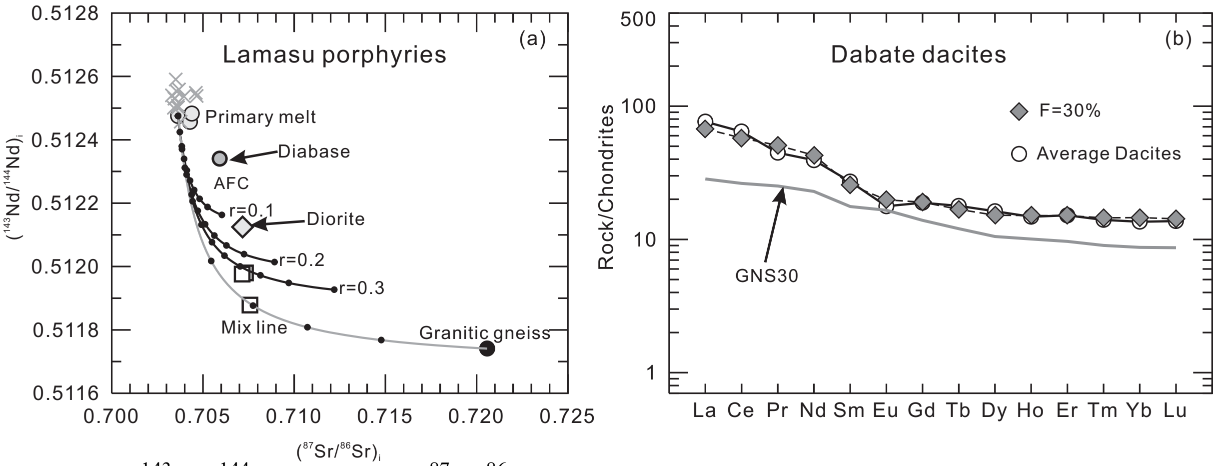

Fig. 12. $(^{143}Nd/^{144}Nd)_i$ versus $(^{87}Sr/^{86}Sr)_i$ plot showing two-component mixing and AFC calculations for Lamasu porphyries. For AFC trends with r = 0.1, 0.2 and 0.3, symbols represent fraction of melt (F) increments of 0.2 but are terminated at F = 0.1. Primary melt from a gabbro sample in the Bayingou ophiolites (Xu et al., 2006a). Data for granitic gneiss of basement rock, southern Wenquan city are form Hu et al. (2000). The bulk partition coefficient for Sr and Nd is 1.12 and 0.13, respectively. (b) REE modeling patterns for Dabate dacites showing melt curves by batch partial melting. The partial coefficients for REEs are from McKenzie and O'Nions, (1991).

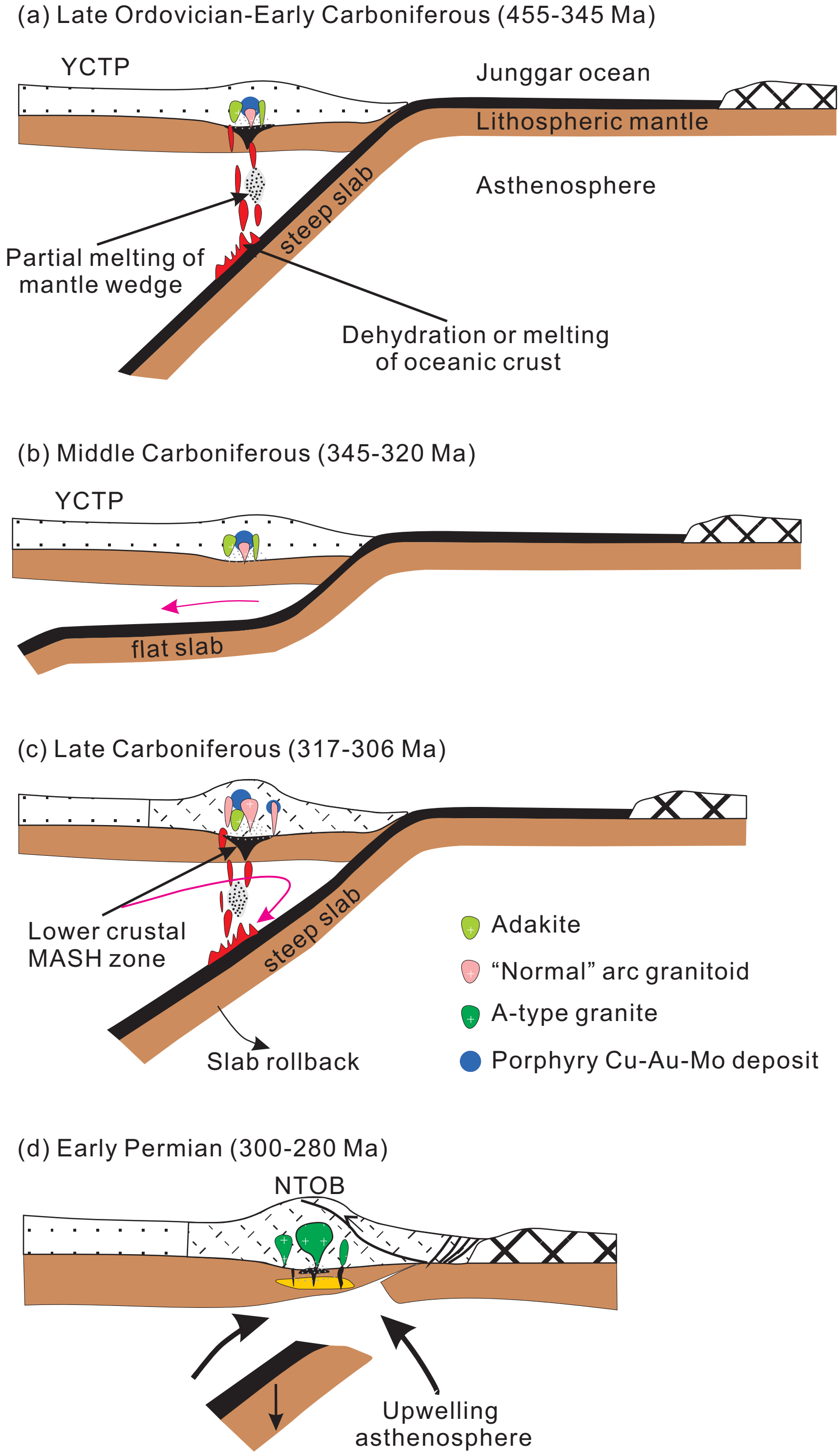

1268

1269 Fig. 13. A suggested model to produce the Late Paleozoic igneous rocks and Cu-Au-Mo deposits
1270 from the northwestern Tianshan Orogenic Belt (NTOB). (a) The Junggar Ocean southward
1271 subducted beneath the Yili-Central Tianshan plate (YCTP) as early as the Late Ordovician (~

455 Ma), and forming the northwestern Tianshan magmatism arc from the Late Devonian to Early Carboniferous (366-345 Ma). We have shown above that the most primitive members of the Lamasu suite already possessed adakitic geochemical traits, and did not acquire them through the AFC processes. Partial melts of subducted oceanic crust-derived adakitic magmas (e.g., the Lamasu intrusive rocks) are considered to be favorable for the generation of porphyry Cu-Au and hydrothermal ore deposits as suggested by many workers (e.g., Defant and Kepezhinskas, 2001; Defant et al., 2002; Mungall, 2002; Wang et al., 2006b). (b) flat-subduction with little or no magmatism. (c) Transition from flat to normal slab subduction owing to slab rollback. A Late Carboniferous magmatic arc formed (317-306 Ma) and was also related to the southward subduction of the Junggar Ocean beneath the YCTP. During this process, multiple factors, such as an arc tectonic setting, relatively oxidized magmas, and AFC - mixing processes at the base of the crust are significant in the generation of giant calc-alkaline porphyry deposits. (d) Slab breakoff: post-collisional environments in the Early Permian NTOB following the disappearance of the Junggar Ocean.

Appendices

Appendix 1 Analytical methods

Zircons were separated using conventional heavy liquid and magnetic separation techniques. Cathodoluminescence (CL) images were obtained for zircons prior to analysis, using a JEOL JXA-8100 Superprobe at the Guangzhou Institute of Geochemistry, Chinese Academy of Sciences (GIGCAS), in order to characterize internal structures and choose potential target sites for U-Pb dating. LA-ICP-MS zircon U–Pb analyses were conducted on an Agilent 7500 ICP-MS equipped with a 193-nm laser, housed at the State Key Laboratory of Geological Processes and Mineral Resources, Faculty of Earth Sciences, China University of Geosciences (Wuhan). Zircon 91500 was used as the standard (Wiedenbeck et al., 1995) and the standard silicate glass NIST 610 was used to optimize the machine, with a beam diameter of 30μm. Raw count rates for ^{29}Si, ^{204}Pb, ^{206}Pb, ^{207}Pb, ^{208}Pb, ^{232}Th and ^{238}U were collected and U, Th and Pb concentrations were calibrated using ^{29}Si as the internal calibrant and NIST 610 as the reference material. $^{207}Pb/^{206}Pb$ and $^{206}Pb/^{238}U$ ratios were calculated using the GLITTER program (Jackson et al., 2004). Measured $^{207}Pb/^{206}Pb$, $^{206}Pb/^{238}U$ and $^{208}Pb/^{232}Th$ ratios in zircon 91500 were averaged over the course of the analytical session and used to calculate correction factors. These correction factors were then applied to each sample to correct for both instrumental mass bias and depth-dependent elemental and isotopic fractionation. Common Pb was corrected by ComPbCorr#3 151 (Andersen, 2002) for those with common ^{206}Pb > 1%. Further detailed descriptions of the instrumentation and analytical procedure for the LA-ICP-MS zircon U-Pb technique can be found in Gao et al., (2002) and Liu et al., (2008, 2010). Uncertainties in the ages listed in Appendix 1 are cited as 1σ, and the weighted mean ages are quoted at the 95% confidence level. The age calculations and concordia plots were made using Isoplot (ver 3.0) (Ludwig, 2003). LA-ICP-MS U–Pb zircon data are presented in Appendix 1.

Major element oxides were determined by standard X-ray fluorescence (XRF). The detailed analytical methods were described by Li et al., (2006). Trace elements were analyzed by inductively coupled plasma mass spectrometry (ICP-MS), using a Perkin-Elmer Sciex ELAN 6000 instrument at GIGCAS. Analytical procedures are similar to those described by Li et al., (2006). Analytical precision for most elements is better than 3%. Results are listed in Appendix 2.

Sr and Nd isotopic analyses were performed on a Micromass Isoprobe multi-collector ICPMS at the GIGCAS, using analytical procedures described by Li et al., (2006). Sr and REE were separated using cation columns, and Nd fractions were further separated by HDEHP-coated Kef columns. Measured $^{87}Sr/^{86}Sr$ and $^{143}Nd/^{144}Nd$ ratios were normalized to $^{86}Sr/^{88}Sr$= 0.1194 and $^{146}Nd/^{144}Nd$=0.7219, respectively. The reported $^{87}Sr/^{86}Sr$ and $^{143}Nd/^{144}Nd$ ratios were adjusted to the NBS SRM 987 standard $^{87}Sr/^{86}Sr$=0.71025 and the Shin Etsu JNdi-1 standard $^{143}Nd/^{144}Nd$=0.512115.

For Pb isotopic determinations, about 100 mg powder was weighed into the Teflon beaker, spiked and dissolved in concentrated HF at 180 °C for 7 h. Lead was separated and purified by conventional cation-exchange technique (AG1× 8, 20-400 resin) with diluted HBr as an eluant. Total procedural blanks were less than 50pg Pb. Isotopic ratios were measured by a VG-354 mass-spectrometer at the GIGCAS. Repeated analyses of SRM 981 yielded average values of $^{206}Pb/^{204}Pb = 16.9 \pm 4$ (2σ), $^{207}Pb/^{204}Pb = 15.498 \pm 4$ (2σ) and $^{208}Pb/^{204}Pb = 36.728 \pm 9$ (2σ). External precisions are estimated to be less than 0.005 and 0.0015. The detailed analytical procedure is similar to those described by Zhu et al., (2001).

In situ zircon Hf isotopic analyses were conducted using a Neptune MC–ICPMS, equipped with a 193-nm laser, at the Institute of Geology and Geophysics, Chinese Academy of Sciences in Beijing, China. During analyses, spot sizes of 32 and 63 mu, with a laser repetition rate of 10 Hz at 100 mJ, were used and raw count rates for ^{172}Yb, ^{173}Yb, ^{175}Lu, $^{176}(Hf + Yb + Lu)$, ^{177}Hf, ^{178}Hf, ^{179}Hf, ^{180}Hf and ^{182}W were collected. During laser ablation analyses, the isobaric interference of ^{176}Lu on ^{176}Hf is negligible due to the extremely low $^{176}Lu/^{177}Hf$ in zircon (normally < 0.002). However, the interference of ^{176}Yb on ^{176}Hf must be carefully corrected since the contribution of ^{176}Yb to ^{176}Hf could profoundly affect the accuracy of the measured $^{176}Hf/^{177}Hf$ ratio. In this project, the mean $^{173}Yb/^{171}Yb$ ratio of the individual spots was used to calculate the fractionation coefficient (β_{Yb}), and then to calculate the contribution of ^{176}Yb to ^{176}Hf. During analysis, an isotopic ratio of $^{176}Yb/^{172}Yb = 0.5887$ was applied. The detailed analytical technique is described in Wu et al., (2006). During the analytical period, the $^{176}Hf/^{177}Hf$ and $^{176}Lu/^{177}Hf$ ratios of the standard zircon (91500) were 0.282294±15 ($2\sigma_n$, n = 20) and 0.00031, similar to the low peaks of

^{176}Hf/^{177}Hf ratios of 0.282284±22 measured by Griffin et al., (2006), also using the laser method.

References

Andersen, T. 2002. Correction of common lead in U-Pb analyses that do not report ^{204}Pb. Chemical Geology 192, 59-79.

Gao, S., Liu, X.M., Yuan, H.L., Hattendorf, B., Günther, D., Chen, L., and Hu, S.H., 2002. Determination of forty two major and trace elements in USGS and NIST SRM glasses by laser ablationinductively coupled plasma-mass spectrometry. Geostand Newsl 26, 181-195.

Griffin, W.L., Pearson, N.J., Belousova, E.A., and Saeed, A., 2006. Comment: Hf-isotope heterogeneity in zircon 91500. Chemical Geology 233(3-4), 358-363.

Jackson, S.E., Pearson, N.J., Belousova, E. and Griffin, W.L., (2004) The application of laser ablation-inductively coupled plasma-mass spectrometry (LA-ICP-MS) to in situ U-Pb geochronology. Chemical Geology 211, 47-69.

Li, X.H., Li, Z.X., Wingate, M.T.D., Chung, S.L., Liu, Y., Lin, G.C., and Li, W.X., 2006. Geochemistry of the 755Ma Mundine Well dyke swarm, northwestern Australia: Part of a Neoproterozoic mantle superplume beneath Rodinia? Precambrian Research 146(1-2), 1-15.

Liu, Y.S., Gao, S., Gao, C.G., Wang, D.B., Zong, K.Q. and Hu, Z.C., 2010. Timing of melt-peridotite interactions in xenoliths of the Trans-North China Orogen: U-Pb dating, Hf isotopes and trace elements in zircon. Journal of Petrology, 51(1-2):537-571.

Liu,Y.S., Hu, Z.C., Gao, S., Günther, D., Xu, J., Gao, C.G. and Chen, H.H., (2008) In situ analysis of major and trace elements of anhydrous minerals by LA-ICP-MS without applying an internal standard. Chemical Geology 257, 34–43.

Ludwig, K.R., 2003. User's manual for Isoplot 3.00: a geochronological toolkit for Microsoft Excel. Berkeley Geochronology Center Special Publication 4, 1–70.

Wiedenbeck, M., Allé, P., Corfu, F., Griffin, W.L., Meier, M., Oberli, F., Von Quadt, A., Roddick, J.C., and Spiegel, W., 1995 Three natural zircon standards for U–Th–Pb, Lu–Hf, trace element and REE analyses. Geostand Newsl 19, 1-23.

Wu, F.Y., Yang, Y.H., Xie, L.W., Yang, J.H. and Xu, P., 2006. Hf isotopic compositions of the standard zircons and baddeleyites used in U-Pb geochronology. Chemical Geology 234(1-2), 105-126.

Zhu, B., Zhang, J., Tu, X., Chang, X., Fan, C., Liu, Y., and Liu, J., 2001. Pb, Sr, and Nd isotopic features in organic matter from China and their implications for petroleum generation and migration. Geochimica et Cosmochimica Acta 65(15), 2555-2570.

Appendix 2 LA-ICP-MS zircon U-Pb isotopic analyses for the magmatic rocks from the Lamasu–Dabate area

Analysis	Content (ppm)		Th/U	Isotopic ratios						Isotopic ages(Ma)					
	Th	U		$^{207}Pb/^{206}Pb$	1σ	$^{207}Pb/^{235}U$	1σ	$^{206}Pb/^{238}U$	1σ	$^{207}Pb/^{206}Pb$	1σ	$^{207}Pb/^{235}U$	1σ	$^{206}Pb/^{238}U$	1σ
Lamasu															
06XJ17-1	252	558	0.45	0.05491	0.00098	0.44026	0.00789	0.05815	0.00066	409	21	370	6	364	4
06XJ17-2	191	676	0.28	0.05564	0.00074	0.44871	0.00616	0.05849	0.00064	438	14	376	4	366	4
06XJ17-3	171	602	0.28	0.05543	0.00079	0.44953	0.00657	0.05882	0.00065	430	15	377	5	368	4
06XJ17-4	399	875	0.46	0.05491	0.00072	0.44436	0.00601	0.05869	0.00064	409	14	373	4	368	4
06XJ17-5	207	526	0.39	0.05520	0.00088	0.49318	0.00798	0.06480	0.00073	420	18	407	5	405	4
06XJ17-6	317	298	1.07	0.05397	0.00087	0.43654	0.00715	0.05867	0.00066	370	18	368	5	368	4
06XJ17-7	338	761	0.44	0.05505	0.00077	0.44136	0.00635	0.05815	0.00064	414	15	371	4	364	4
06XJ17-8	399	655	0.61	0.05395	0.00076	0.43456	0.00626	0.05842	0.00065	369	15	366	4	366	4
06XJ17-9	123	256	0.48	0.05580	0.00100	0.45052	0.00813	0.05856	0.00067	444	21	378	6	367	4
06XJ17-10	386	930	0.41	0.05483	0.00077	0.44615	0.00648	0.05902	0.00065	405	15	375	5	370	4
06XJ17-11	149	285	0.52	0.05620	0.00104	0.45087	0.00838	0.05818	0.00067	460	22	378	6	365	4
06XJ17-12	153	620	0.25	0.05343	0.00124	0.43225	0.00886	0.05867	0.00065	347	54	365	6	368	4
06XJ17-13	133	336	0.40	0.05502	0.00087	0.44098	0.00707	0.05813	0.00065	413	18	371	5	364	4
06XJ17-14	220	573	0.38	0.05589	0.00095	0.49558	0.00853	0.06431	0.00073	448	19	409	6	402	4
06XJ17-15	245	455	0.54	0.05474	0.00083	0.44193	0.00685	0.05855	0.00066	402	17	372	5	367	4
06XJ17-16	295	630	0.47	0.05477	0.00083	0.44530	0.00691	0.05897	0.00066	403	17	374	5	369	4
06XJ17-17	114	329	0.35	0.05551	0.00099	0.49000	0.00881	0.06403	0.00073	433	21	405	6	400	4
06XJ17-18	143	366	0.39	0.05442	0.00088	0.43387	0.00714	0.05782	0.00065	388	18	366	5	362	4
06XJ17-19	30	262	0.12	0.06911	0.00116	1.41784	0.02419	0.14880	0.00171	902	18	896	10	894	10
06XJ17-20	282	715	0.39	0.06625	0.00097	1.10806	0.01657	0.12131	0.00136	814	15	757	8	738	8
06XJ17-21	311	732	0.42	0.06893	0.00100	1.33419	0.01980	0.14039	0.00158	897	14	861	9	847	9
06XJ17-22	255	889	0.29	0.05407	0.00086	0.43435	0.00701	0.05826	0.00066	374	18	366	5	365	4
06XJ17-23	48	312	0.15	0.05670	0.00099	0.45608	0.00803	0.05834	0.00067	480	20	382	6	366	4
06XJ17-24	462	950	0.49	0.06905	0.00103	1.43796	0.02192	0.15104	0.00170	900	15	905	9	907	10
Dabate dacite															
06XJ04 01	329	409	0.80	0.05537	0.00203	0.51241	0.01784	0.06714	0.00097	427	52	420	12	419	6
06XJ04 02	127	165	0.77	0.05693	0.00373	0.39931	0.02499	0.05087	0.00110	489	100	341	18	320	7
06XJ04 03	147	141	1.04	0.05157	0.00367	0.35842	0.02445	0.05041	0.00114	266	115	311	18	317	7
06XJ04 04	357	366	0.97	0.06736	0.00288	0.62669	0.02523	0.06747	0.00117	849	55	494	16	421	7
06XJ04 05	176	339	0.52	0.07172	0.00152	1.60833	0.03168	0.16263	0.00182	978	22	973	12	971	10

Appendix 2 Continued

Analysis	Content (ppm)		Th/U	Isotopic ratios						Isotopic ages(Ma)					
	Th	U		$^{207}Pb/^{206}Pb$	1σ	$^{207}Pb/^{235}U$	1σ	$^{206}Pb/^{238}U$	1σ	$^{207}Pb/^{206}Pb$	1σ	$^{207}Pb/^{235}U$	1σ	$^{206}Pb/^{238}U$	1σ
06XJ04 06	256	680	0.38	0.06944	0.0019	1.22167	0.03138	0.12759	0.00165	912	32	811	14	774	9
06XJ04 07	95	127	0.75	0.05378	0.00437	0.37927	0.02959	0.05115	0.00131	362	130	327	22	322	8
06XJ04 08	78	104	0.75	0.05795	0.00473	0.40011	0.03122	0.05007	0.00135	528	124	342	23	315	8
06XJ04 09	149	153	0.97	0.05442	0.00767	0.36992	0.05005	0.04929	0.00215	388	224	320	37	310	13
06XJ04 10	214	327	0.66	0.0472	0.0031	0.32256	0.02036	0.04956	0.00103	59	99	284	16	312	6
06XJ04 11	68	150	0.45	0.05476	0.00486	0.39093	0.0332	0.05176	0.00150	402	139	335	24	325	9
06XJ04 12	1645	1246	1.32	0.07089	0.00231	0.48748	0.01483	0.04985	0.00070	954	39	403	10	314	4
Dabate granite															
06XJ013-1	61	105	0.58	0.05397	0.00238	0.37540	0.01586	0.05045	0.00064	370	102	324	12	317	4
06XJ013-2	193	358	0.54	0.07118	0.00116	0.45377	0.00749	0.04623	0.00052	963	17	380	5	291	3
06XJ013-3	146	290	0.50	0.05402	0.00166	0.34298	0.00980	0.04604	0.00053	372	71	299	7	290	3
06XJ013-4	302	509	0.59	0.05359	0.00072	0.34155	0.00473	0.04622	0.00051	354	14	298	4	291	3
06XJ013-5	29	61	0.48	0.05311	0.00138	0.33785	0.00873	0.04614	0.00056	333	37	296	7	291	3
06XJ013-6	79	155	0.51	0.05310	0.00196	0.37170	0.01301	0.05077	0.00061	333	86	321	10	319	4
06XJ013-7	50	175	0.28	0.05339	0.00099	0.33923	0.00633	0.04609	0.00052	345	23	297	5	290	3
06XJ013-8	356	677	0.53	0.05327	0.00077	0.33625	0.00501	0.04578	0.00050	340	16	294	4	289	3
06XJ013-9	324	545	0.59	0.05314	0.00070	0.34021	0.00466	0.04643	0.00051	335	14	297	4	293	3
06XJ013-10	455	615	0.74	0.06762	0.00272	0.41114	0.01572	0.04410	0.00055	857	86	350	11	278	3
06XJ013-11	106	190	0.56	0.05341	0.00107	0.37410	0.00751	0.05079	0.00058	346	25	323	6	319	4
06XJ013-12	137	221	0.62	0.05675	0.00093	0.36120	0.00599	0.04616	0.00051	482	19	313	4	291	3
06XJ013-13	256	317	0.81	0.05244	0.00077	0.33593	0.00504	0.04646	0.00051	305	16	294	4	293	3
06XJ013-14	850	1616	0.53	0.06358	0.00600	0.33191	0.03097	0.03786	0.00054	728	208	291	24	240	3
06XJ013-15	65	169	0.38	0.05196	0.00094	0.33400	0.00612	0.04662	0.00053	284	22	293	5	294	3
06XJ013-16	89	167	0.53	0.05841	0.00238	0.35907	0.01394	0.04458	0.00056	545	91	312	10	281	3
06XJ013-17	645	1253	0.51	0.06261	0.00092	0.36572	0.00551	0.04236	0.00047	695	15	316	4	267	3
06XJ013-18	139	499	0.28	0.05614	0.00079	0.39290	0.00569	0.05075	0.00056	458	15	336	4	319	3
06XJ013-19	669	663	1.01	0.06496	0.00090	0.40648	0.00580	0.04538	0.00050	773	14	346	4	286	3
06XJ013-20	290	460	0.63	0.05735	0.00200	0.35351	0.01162	0.04470	0.00052	505	79	307	9	282	3
06XJ013-22	199	414	0.48	0.06178	0.00091	0.39809	0.00600	0.04673	0.00052	667	15	340	4	294	3
06XJ013-23	349	644	0.54	0.05353	0.00078	0.34120	0.00509	0.04622	0.00051	351	16	298	4	291	3
06XJ013-24	178	365	0.49	0.05154	0.00161	0.32488	0.00942	0.04572	0.00053	265	73	286	7	288	3
06XJ013-25	139	383	0.36	0.05433	0.00080	0.34127	0.00515	0.04556	0.00050	385	16	298	4	287	3

Appendix 3 Major and trace element data for the magmatic rocks from the Lamasu–Dabate area

Sample	06XJ-16	06XJ-017	06XJ-018	06XJ-19-1	06XJ-19-2	06XJ-20	06XJ-21-1	06XJ-22	06XJ-23-1	06XJ-23-2
Location	Lamasu	Lamasu	Lamasu	Lamasu	Lamasu	Lamasu	Lamasu	Lamasu	Lamasu	Lamasu
SiO2	67.86	66.85	50.66	58.30	55.89	69.46	68.33	59.70	68.23	67.25
TiO2	0.30	0.31	1.75	1.21	1.40	0.25	0.30	0.38	0.34	0.34
Al2O3	16.67	16.59	16.79	16.25	16.88	16.04	17.06	19.75	16.47	16.46
FeO	1.22	2.45	8.52	5.91	6.50	0.84	1.90	2.56	2.80	3.05
MnO	0.01	0.02	0.14	0.06	0.07	0.02	0.01	0.02	0.05	0.05
MgO	0.88	1.28	5.81	3.38	3.73	0.75	1.37	1.69	1.16	1.23
CaO	0.47	2.57	7.68	2.72	3.02	2.00	0.84	1.77	2.63	2.84
Na2O	2.49	3.50	3.15	3.32	2.61	4.79	4.24	6.52	4.06	4.33
K2O	7.53	4.05	1.37	3.35	3.61	4.54	3.56	3.62	2.14	1.78
P2O5	0.06	0.03	0.13	0.27	0.31	0.05	0.05	0.10	0.04	0.04
LOI	1.96	1.56	2.72	4.43	5.45	1.19	2.16	2.94	1.85	1.74
Total	99.60	99.48	99.66	99.84	100.19	100.03	100.04	99.34	100.09	99.44
Mg#	56.21	48.23	54.83	50.42	50.56	61.20	56.33	54.02	42.43	41.85
Sc	4.13	0.721	20.8	10.5	13.3	2.74	2.61	3.69	2.59	2.81
V	19.8	25.6	144	99.1	130	25.3	26.0	42.9	38.0	31.0
Cr	20.3	11.9	188	23.3	32.2	11.4	11.0	6.74	7.65	29.0
Co	1.36	4.41	29.4	13.9	16.6	0.680	3.22	3.60	5.50	4.92
Ni	5.44	9.22	38.7	20.2	21.6	6.91	9.69	7.31	7.06	8.43
Ga	15.2	13.7	18.5	18.8	19.2	13.6	17.5	16.7	16.6	16.2
Cs	13.9	4.56	2.30	4.26	5.76	3.50	6.33	7.82	2.28	4.15
Rb	220	92.3	33.3	111	136	103	109	128	67.3	56.3
Ba	509	235	225	328	297	433	337	347	353	257
Th	8.09	3.13	3.11	10.4	9.63	7.62	6.88	6.32	7.09	6.88
U	1.09	1.10	0.721	2.11	1.78	1.79	0.954	1.22	1.00	1.28
Pb	5.96	2.91	4.80	11.0	6.74	3.80	8.56	7.01	5.80	6.04
Nb	6.26	4.76	9.20	12.4	13.3	8.11	6.43	5.41	6.20	6.30
Ta	0.606	0.456	0.583	0.813	0.866	0.784	0.554	0.488	0.591	0.573
Sr	445	308	420	258	132	383	359	401	436	372
Y	13.7	10.6	21.5	24.4	23.2	16.8	12.8	13.9	15.3	14.5
Zr	123	67.4	245	228	243	109	93.0	130	108	102
Hf	3.23	1.98	5.22	5.64	5.77	2.99	2.59	3.56	3.16	3.09
La	17.8	9.95	12.9	33.8	33.9	10.2	14.7	18.1	19.0	17.8
Ce	37.7	22.2	29.6	74.0	72.1	26.8	31.0	38.1	38.1	36.8
Pr	4.58	2.83	3.85	8.95	8.95	3.72	3.92	4.85	4.61	4.43
Nd	16.4	10.6	15.7	33.2	33.5	14.7	14.6	17.6	17.1	16.3
Sm	3.06	2.08	3.58	6.01	6.05	3.01	2.75	3.07	3.12	2.94
Eu	0.517	0.435	1.44	0.933	0.959	0.502	0.435	0.611	0.656	0.689
Gd	2.36	1.94	3.56	5.17	5.03	2.62	2.25	2.59	2.65	2.66
Tb	0.403	0.326	0.614	0.803	0.803	0.446	0.366	0.401	0.470	0.415
Dy	2.27	1.91	3.79	4.57	4.24	2.63	2.06	2.29	2.55	2.55
Ho	0.490	0.388	0.805	0.870	0.840	0.550	0.431	0.499	0.521	0.506
Er	1.39	1.12	2.27	2.42	2.24	1.57	1.22	1.40	1.47	1.45
Tm	0.205	0.175	0.351	0.346	0.323	0.234	0.191	0.227	0.227	0.236
Yb	1.42	1.21	2.30	2.16	2.07	1.60	1.26	1.48	1.53	1.56
Lu	0.225	0.184	0.384	0.329	0.318	0.255	0.196	0.239	0.237	0.248

Appendix 3 Continued

Sample	06XJ-04	06XJ-05	06XJ-06	06XJ-08	06XJ-010	06XJ-12	06XJ-13	06XJ-14	06XJ-15
Location	Dabate	Dabate	Dabate	Dabate	Dabate	Dabate	Dabate	Dabate	Dabate
SiO2	63.95	62.18	62.50	75.56	75.67	76.92	76.36	75.38	77.61
TiO2	0.94	0.71	0.66	0.08	0.12	0.09	0.11	0.10	0.10
Al2O3	14.60	15.41	16.02	12.80	12.04	12.91	12.72	12.64	12.97
FeO	5.55	6.38	4.91	1.04	1.02	0.85	1.16	1.05	0.88
MnO	0.05	0.02	0.10	0.00	0.00	0.00	0.00	0.00	0.00
MgO	1.72	2.82	3.25	0.05	0.05	0.01	0.01	0.06	0.01
CaO	3.02	0.33	4.16	0.03	0.03	0.28	0.34	0.42	0.31
Na2O	3.11	3.99	3.17	2.47	1.39	3.00	3.56	4.06	3.27
K2O	3.14	5.53	2.24	7.63	8.08	5.27	5.14	4.92	5.21
P2O5	0.11	0.05	0.09	0.01	0.01	0.01	0.01	0.01	0.00
LOI	2.69	1.50	2.25	0.62	0.88	0.79	0.87	0.79	-0.31
Total	99.49	99.64	99.92	100.40	99.41	100.21	100.40	99.54	100.14
Mg#	35.56	44.07	54.11	7.28	8.67	2.05	1.52	8.75	1.99
Sc	15.3	14.8	10.7	0.121	0.0450	2.19	0.0420	0.849	0.137
V	88.2	102	98.0	9.09	15.6	3.95	7.98	19.6	7.36
Cr	32.2	53.8	66.7	4.20	8.43	15.6	2.51	7.25	12.2
Co	13.5	0.859	17.2	0.424	0.768	0.518	0.625	0.452	0.652
Ni	14.4	39.5	51.7	1.41	2.63	3.06	2.09	1.83	7.61
Ga	18.3	17.0	17.6	20.8	19.8	21.8	22.8	25.2	23.2
Cs	3.95	77.0	4.67	20.0	18.4	15.3	14.5	17.2	18.6
Rb	87.6	459	61.7	316	357	265	264	286	287
Ba	641	476	314	110	209	144	150	107	109
Th	7.57	5.07	4.58	15.4	13.0	20.2	15.3	18.7	12.5
U	1.82	1.26	1.09	3.72	2.92	3.38	2.38	2.50	7.44
Pb	10.7	4.97	8.23	9.52	6.15	10.1	9.80	14.4	12.5
Nb	8.73	7.21	6.89	25.2	20.6	24.8	25.6	27.5	24.2
Ta	0.496	0.432	0.425	2.29	1.82	2.18	2.04	2.28	2.10
Sr	213	208	394	35.1	29.3	22.8	27.1	18.6	17.9
Y	38.2	19.9	19.3	40.8	29.6	57.3	52.7	58.7	51.5
Zr	277	138	134	91.6	101	140	128	142	121
Hf	5.64	2.96	2.98	4.08	4.05	5.81	5.29	5.83	5.29
La	23.8	7.89	13.2	8.17	6.63	19.1	15.9	18.8	13.3
Ce	52.1	16.9	28.1	22.5	17.3	46.7	37.4	43.9	31.7
Pr	6.64	2.22	3.65	3.23	2.40	6.20	4.90	6.04	4.22
Nd	26.8	8.43	14.4	13.6	10.5	23.6	18.5	23.1	15.9
Sm	5.80	1.97	3.16	4.86	3.35	6.65	5.12	6.42	4.64
Eu	1.03	0.543	0.768	0.145	0.154	0.268	0.211	0.225	0.199
Gd	5.37	1.98	2.98	5.26	3.48	7.84	6.08	7.37	5.97
Tb	0.972	0.414	0.517	1.11	0.710	1.61	1.38	1.59	1.39
Dy	5.81	2.83	2.99	6.76	4.44	10.1	8.70	9.62	8.74
Ho	1.20	0.624	0.635	1.39	0.923	2.11	1.78	2.07	1.86
Er	3.42	1.86	1.73	3.74	2.64	5.94	5.06	5.76	5.28
Tm	0.508	0.295	0.262	0.575	0.428	0.919	0.729	0.873	0.787
Yb	3.07	1.86	1.65	3.67	2.73	5.80	4.78	5.47	4.87
Lu	0.466	0.277	0.232	0.517	0.409	0.887	0.687	0.788	0.720

Appendix 4 Sr, Nd and Pb isotopic compositions for the magmatic rocks from the Lamasu–Dabate area

Sample	T(Ma)	Rb(ppm)	Sr(ppm)	$^{87}Rb/^{86}Sr$	$^{87}Sr/^{86}Sr$	2σ	$^{87}Sr/^{86}Sr_i$	Sm	Nd	$^{147}Sm/^{144}Nd$	$^{143}Nd/^{144}Nd$	2σ
06XJ017	366	92.34	308.3	0.844659	0.711848	5	0.707446	2.082	10.6	0.119544	0.5122663	6
06XJ018	366	33.28	420	0.223460	0.707117	5	0.705952	3.575	15.66	0.138943	0.5126735	5
06XJ19-2	366	135.7	131.9	2.901350	0.711690	8	0.696572	6.054	33.48	0.110055	0.5125016	6
06XJ20	366	102.5	382.7	0.755319	0.711619	5	0.707683	3.013	14.69	0.124833	0.5121772	5
06XJ22	366	127.5	401.2	0.896219	0.711962	5	0.707292	3.071	17.64	0.105958	0.5123794	6
06XJ23-2	366	56.33	371.5	0.427608	0.709432	5	0.707204	2.938	16.29	0.109770	0.5122389	6
06XJ04	316	87.56	213.20	1.158200	0.710678	14	0.705469	5.804	26.8	0.130495	0.5126721	9
06XJ06	316	61.73	393.70	0.442177	0.706593	9	0.704604	3.164	14.44	0.137374	0.5125097	7
06XJ010	290	356.5	29.25					3.352	10.46	0.195041	0.512635	6
06XJ13	290	264.2	27.14					5.117	18.47	0.168617	0.5125342	6
06XJ15	290	286.9	17.87					4.638	15.86	0.177984	0.5125141	5

Sample	εNd(t)	T_{Nd2DM}	$f_{Sm/Nd}$	Th(ppm)	U(ppm)	Pb(ppm)	$^{206}Pb/^{204}Pb$	$^{207}Pb/^{204}Pb$	$^{208}Pb/^{204}Pb$	$^{206}Pb/^{204}Pb_t$	$^{207}Pb/^{204}Pb_t$	$^{208}Pb/^{204}Pb_t$
06XJ017	-3.65	1423	-0.39	3.129	1.095	2.907	19.806	15.628	39.449	18.139	15.5381	37.9483
06XJ018	3.40	847	-0.29	3.109	0.721	4.799	18.694	15.651	38.634	18.0458	15.616	37.7534
06XJ19-2	1.39	1011	-0.44	9.632	1.782	6.741	19.068	15.618	39.491	17.909	15.5555	37.5173
06XJ20	-5.63	1585	-0.37	7.615	1.789	3.796	20.241	15.659	39.389	18.1442	15.5459	36.5771
06XJ22	-0.80	1191	-0.46	6.316	1.216	7.013	19.206	15.622	38.981	18.4495	15.5812	37.7431
06XJ23-2	-3.72	1430	-0.44	6.88	1.28	6.044	19.371	15.598	39.246	18.442	15.5479	37.6729
06XJ04	3.29	815	-0.33									
06XJ06	0.05	1080	-0.32									
06XJ010	0.00	1062	-0.01	13.03	2.918	6.154	20.228	15.803	39.567	18.5689	15.7165	37.2233
06XJ13	-0.99	1143	-0.14	15.27	2.375	9.799	19.562	15.758	39.632	18.7211	15.7142	37.9216
06XJ15	-1.72	1204	-0.10									

Appendix 5 Zircon Lu-Hf isotopic compositions for the porphyries from the Lamasu–Dabate area

Spot	$^{176}Yb/^{177}Hf$	$^{176}Lu/^{177}Hf$	$^{176}Hf/^{177}Hf$	±2σ	T(Ma)	(176Hf/177Hf)i	εHf(t)	TDM (Ga)	*f*Lu/Hf
Lamasu (06XJ17)									
06XJ17H1	0.04154	0.001737	0.282736	0.000027	364	0.282724558	6.3	0.75	-0.95
06XJ17H2	0.03410	0.001428	0.282651	0.000029	366	0.282641163	3.4	0.86	-0.96
06XJ17H6	0.03806	0.001542	0.282733	0.000026	368	0.282722208	6.3	0.75	-0.95
06XJ17H7	0.05288	0.002157	0.282618	0.000024	364	0.282602845	2.0	0.93	-0.94
06XJ17H8	0.05041	0.002018	0.282626	0.000032	366	0.282612212	2.4	0.91	-0.94
06XJ17H9	0.03963	0.001730	0.282666	0.000025	367	0.282654159	3.9	0.85	-0.95
06XJ17H10	0.08466	0.003326	0.282865	0.000037	370	0.282841811	10.6	0.58	-0.90
06XJ17H11	0.04498	0.001877	0.282789	0.000033	365	0.282775818	8.2	0.67	-0.94
06XJ17H12	0.04177	0.001737	0.282630	0.000021	368	0.282618308	2.7	0.90	-0.95
06XJ17H13	0.03805	0.001591	0.282598	0.000023	364	0.282587445	1.5	0.94	-0.95
06XJ17H15	0.03732	0.001575	0.282594	0.000023	367	0.28258342	1.4	0.95	-0.95
06XJ17H16	0.02806	0.001204	0.282631	0.000017	369	0.282622449	2.8	0.88	-0.96
06XJ17H18	0.04524	0.001906	0.282784	0.000028	362	0.282770779	7.9	0.68	-0.94
06XJ17H22	0.03707	0.001564	0.282613	0.000023	365	0.282601891	2.0	0.92	-0.95
06XJ17H23	0.03221	0.001350	0.282633	0.000022	366	0.282623612	2.8	0.88	-0.96
06XJ17H5	0.02715	0.001152	0.282574	0.000025	405	0.282564837	1.6	0.96	-0.97
06XJ17H17	0.04366	0.001800	0.282606	0.000028	400	0.282592637	2.5	0.93	-0.95
06XJ17H24	0.03307	0.001275	0.282342	0.000020	907	0.282320586	4.1	1.29	-0.96
06XJ17H19	0.03502	0.001381	0.282279	0.000021	894	0.282255474	1.5	1.39	-0.96
06XJ17H20	0.03759	0.001540	0.282529	0.000026	738	0.282508092	7.0	1.04	-0.95
06XJ17H21	0.02583	0.001060	0.282411	0.000020	847	0.282393817	5.3	1.19	-0.97
Dabate (06XJ13)									
06XJ13H2	0.06174	0.002198	0.282755	0.000026	291	0.282743366	5.4	0.73	-0.93
06XJ13H4	0.04701	0.001738	0.282751	0.000023	291	0.282741504	5.3	0.72	-0.95
06XJ13H5	0.02733	0.001081	0.282743	0.000021	291	0.282736778	5.2	0.72	-0.97
06XJ13H7	0.03285	0.001225	0.282712	0.000024	290	0.282705175	4.0	0.77	-0.96
06XJ13H9	0.03537	0.001313	0.282773	0.000025	293	0.28276565	6.2	0.68	-0.96
06XJ13H10	0.07640	0.002731	0.282730	0.000024	278	0.282715352	4.1	0.78	-0.92
06XJ13H12	0.03357	0.001331	0.282777	0.000026	291	0.282769521	6.3	0.68	-0.96
06XJ13H13	0.05890	0.002212	0.282704	0.000025	293	0.282691566	3.6	0.80	-0.93
06XJ13H15	0.03367	0.001349	0.282730	0.000022	294	0.282722835	4.7	0.75	-0.96
06XJ13H19	0.09805	0.003514	0.282732	0.000025	286	0.282712966	4.2	0.79	-0.89
06XJ13H20	0.05437	0.001933	0.282779	0.000025	282	0.282768607	6.1	0.69	-0.94
06XJ13H22	0.04366	0.001703	0.282613	0.000022	294	0.282603968	0.5	0.92	-0.95
06XJ13H23	0.05299	0.001977	0.282781	0.000025	291	0.282770158	6.3	0.69	-0.94
06XJ13H24	0.04036	0.001489	0.282863	0.000039	288	0.282855456	9.3	0.56	-0.96
06XJ13H25	0.06987	0.002334	0.282740	0.000039	287	0.282727885	4.8	0.75	-0.93
06XJ13H6	0.02555	0.001017	0.282681	0.000025	319	0.282675263	3.6	0.81	-0.97
06XJ13H18	0.06421	0.002400	0.282721	0.000030	319	0.282706231	4.7	0.78	-0.93
06XJ13H11	0.03908	0.001686	0.282915	0.000024	319	0.282904464	11.7	0.49	-0.95